Automatic Segmentation and Classification of Multiple Sclerosis Lesions Using Quantitative Magnetic Resonance Imaging

Johanna Alfredsson

LiU LINKÖPING UNIVERSITY

Master of Science Thesis in Biomedical Engineering

Automatic Segmentation and Classification of Multiple Sclerosis Lesions Using Quantitative Magnetic Resonance Imaging

Johanna Alfredsson

LIU-IMT-TFK-A—19/561—SE

Supervisor: **PhD student Anette Karlsson**
IMT, Linköping University
M.Sc. Catharina Petersén
SyntheticMR

Examiner: **Professor Magnus Borga**
IMT, Linköping University

Department of Biomedical Engineering
Linköping University
SE-581 83 Linköping, *Sweden*

Abstract

Multiple sclerosis is a neurological disease causing a degeneration of myelin around the axons in the central nervous system. This process leaves traces in the form of lesions, which can be distinguished in an MRI examination. It is important to detect these at an early stage to state diagnosis and initiate medication.

In this Master's Thesis, an automatic segmentation algorithm was developed, with the purpose of segmenting possible multiple sclerosis lesions. Secondly, a progression model was developed with the purpose of estimating the state of each individual lesion. The implementation was based on synthetic contrast weighted images, segmentation maps and quantitative relaxation maps produced by SyMRI (SyntheticMR, Linköping, Sweden).

The automatic segmentation algorithm has a relatively high sensitivity but low precision, causing a large number of false positives. The algorithm performed better in the cerebrum compared to the cerebellum. The large number of false positives appeared mainly due to partial volume effects, creating hyperintense artifacts in synthetic T2W FLAIR images. A larger amount of data would have been desirable to create a more robust algorithm.

The progression model showed promising results, with a clear correlation to the synthetic contrast-weighted images and segmentation maps available in SyMRI. The progression model could be useful in disease monitoring, medical decisions and diagnosis of Multiple Sclerosis.

Acknowledgments

Contents

Notation

Abbreviations	Meaning
BBB	Blood–brain barrier
CNS	Central nervous system
CSF	Cerebrospinal fluid
DMT	Disease-modifying therapies
DSC	Dice similarity coefficient
FLAIR	Fluid-attenuated inversion recovery
FN	False negative
FP	False positive
GM	Gray matter
MRI	Magnetic resonance imaging
MS	Multiple sclerosis
PD	Proton density
PPMS	Primary progressive multiple sclerosis
PPV	Positive predictive value
PSIR	Phase sensitive inversion recovery
qMRI	Quantitative magnetic resonance imaging
RF	Radio frequency
RRMS	Relapsing–remitting multiple sclerosis
R1	Spin-lattice relaxation rate
R2	Spin-spin relaxation rate
SPMS	Secondary progressive multiple sclerosis
TE	Echo time
TI	Inversion time
TN	True negative
TP	True positive
TPR	True positive rate
TR	Repetition time
T1	Spin-lattice relaxation time
T2	Spin-spin relaxation time
WM	White matter

1

Introduction

This report is the final result of a Master's Thesis within the field of Biomedical Engineering performed at Linköping University, in collaboration with SyntheticMR AB (Linköping, Sweden). In this chapter, a short background is presented together with the purpose and limitations of this work.

1.1 Background

Multiple Sclerosis (MS) is an autoimmune disease that causes degeneration of myelin in the central nervous system (CNS). This causes inflammation and tissue destruction, which can be distinguished by magnetic resonance imaging (MRI), which is used to diagnose the disease [1]. It is important to state an early diagnosis since it has been proven that medication is most effective during the early stages of the disease [2].

The MR images are studied manually, searching for radiological abnormalities that can confirm the diagnosis. However, there are many factors that can cause the radiologist to miss such abnormalities, such as fatigue, insufficient communication, lack of concentration or unintentional blindness. It can therefore be motivated to assist the radiologist with computer-aided detection, so that vague lesions are not overseen [3].

Furthermore, there are no restrictions that state how a manual segmentation should be performed, leading to different segmentation results between individuals. In Figure 1.1 it is seen how the same area is segmented differently, not only causing a great diversity in lesion area, but in this case also affecting the total number of lesions. The differences can be problematic when examining how lesions change over time, since it is a question of interpretation. This would not

be a problem if computer-aided segmentation was used, eliminating the human factor and preference.
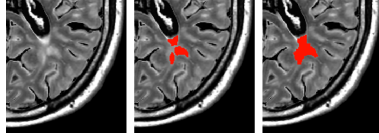
Figure 1.1: Manual segmentation can be highly individual

Examples of MS diagnosed brains can be seen in Figure 1.2 and 1.3 where the assumed lesions are pointed out by red arrows. When studying the two figures, one can see that the lesions vary in size, shape and intensity. Lesions appear hyperintense in a T2W FLAIR contrast weighted image and hypointense in a PSIR contrast weighted image. However, these kinds of areas are not necessarily pathological, an example of this can be seen in Figure 1.4, where perivascular spaces are present. These are nonpathological and appear naturally with rising age.
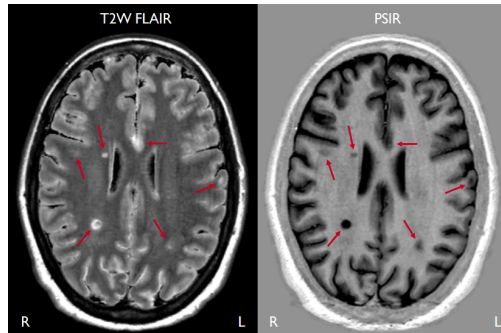
Figure 1.2: A MS diagnosed patient, the red arrows point out the location of the assumed lesions, which vary in intensity, shape and size
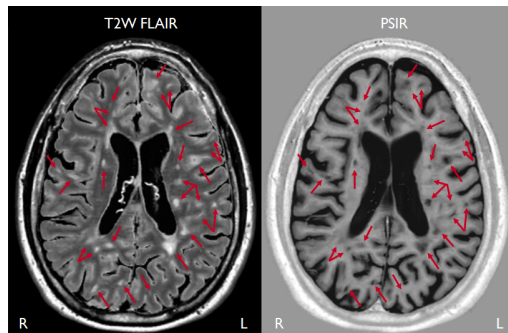
Figure 1.3: A MS diagnosed patient with a wide range of possible lesions
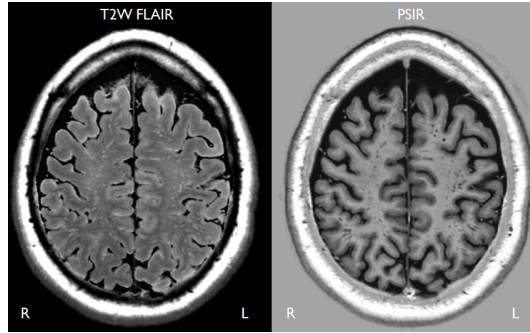
Figure 1.4: *A healthy volunteer, with presence of perivascular spaces, which should not be segmented as MS lesions*

Furthermore, it could be useful for the radiologist to know the state of progression for each individual lesion. This could ease the decision between the various number of treatments available, and could be used as direct feedback if a treatment is sufficient or not, showing stagnation of the progression or re-progression if the tissue is healed.

This Master's Thesis is based on synthetic MRI, which is a simulation method that is used to generate contrast weighted MR images by quantitative MRI (qMRI). The software SyMRI (SyntheticMR, Linköping, Sweden) can generate several contrast-weighted images, parametric maps and different segmentation maps, all based on one single scan [4]. From an image-processing point of view, this is a great advantage, since additional registration steps is not required.

1.2   Purpose

The purpose of this master's thesis is to create an automatic segmentation algorithm for MS lesions, using qMRI data. Secondly, it is investigated if it is possible to differentiate lesions from healthy tissue using quantitative data, and to create a model that classifies lesions based on their progression.

The following two aims have been stated for this master's thesis:

- *Create an algorithm that performs an automatic segmentation of possible MS lesions.*

- *Examine whether any characteristics of MS lesions can be found in the quantitative MR data, and propose a model that classifies these lesions based on their progression.*

1.2.1   Limitations

A lesion is defined as a hyperintense area in a T2W FLAIR image that has a minimum diameter of 3mm [5]. There are many typical locations for MS lesions in the CNS. In this thesis, the focus will be to detect lesions located in white matter, cortical lesions are excluded due to their vague appearance. Lesions located in the spinal cord are not included. The lesions are classified as possible lesions since no radiologist has confirmed the manual segmentation. A white matter hyperintensity detected in a patient with diagnosed MS will be considered as an MS lesion and a white matter hyperintensity detected in a healthy volunteer will be considered nonpathological.

2

Theory

The theory basis of the Master's Thesis is included in this chapter. The background and pathogenesis of Multiple Sclerosis are presented including how the diagnosis is determined using MRI. A description of conventional MRI and synthetic MRI is also included.

2.1 Multiple Sclerosis

Multiple Sclerosis (MS) is a neurological disease that affects the central nervous system (CNS). The disease is mainly detected within the age span of 20-40 years and women are more often affected than men. The prevalence of the disease varies greatly over the world and the highest number of cases is seen in Europe and North America, while it is more uncommon in Africa and East Asia [6]. Today, it is not fully known what triggers the outbreak of the disease, but many studies indicate that it has both genetic and environmental causes. It has been proved that the risk of developing MS increases with increasing distance from the equator [7]. It has been suggested that MS could develop due to different types of viral infections, for example the Epstein-Barr virus, if the person caught the infection as a young adult [7]. Other factors such as smoking have also been suggested to increase the risk of developing MS [8].

2.1.1 Symptoms and Progression

The symptoms of MS vary greatly between individuals, which can complicate the diagnosis of the patient. The most common symptoms are movement and coordination problems, impaired hearing, fatigue and impaired vision. Some people also experiencing bladder issues, sexual dysfunction, cognitive problems and pain [6].

The progression pattern of the disease is divided into the following types:

- **RRMS** - Relapsing–Remitting Multiple Sclerosis

- **SPMS** - Secondary Progressive Multiple Sclerosis

- **PPMS** - Primary Progressive Multiple Sclerosis

Approximately 80-90% of the MS patients initially develop the RRMS type. During this stage, the patient will experience active periods with symptoms, but after some time, the body will undergo a relapsing process where a spontaneous neurological recovery is seen. During the remittance period, the MS patient experiences a full recovery. Many RRMS patients will gradually progress into the SPMS stage, in which the recovery decreases after each attack and gradually increasing the dysfunction of the damaged neurons, see Figure 2.1. The other 10-20% of the MS population develop PPMS, which is characterized by its progressive dysfunctionality and no relapsing activity [9]. The life expectancy is reduced by 5-10 years for a person diagnosed with MS, and it may take many years before developing complete disability [10].
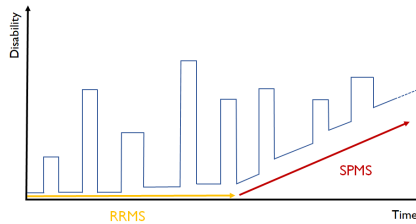
Figure 2.1: An example of the changes in disability during RRMS and SPMS

2.1.2 Anatomy of the Central Nervous System

The communication within the brain and between the rest of the body is controlled by the nerve cell, also called *neuron*, which is illustrated in Figure 2.2. The nucleus of the neuron is found in the cell body where dendrites branch out to nearby axons which have a longer and more robust structure compared with the dendrites. The electrical impulses propagate along the axon and are sent to the following neuron by electrochemical stimulation. Some axons are *myelinated*, which means that they are enclosed by a myelin sheath that is produced by oligodendrocytes. The myelin sheath is a multi-layered lipid- and protein rich substance that insulates the axon, which will increase the signal propagation speed. There are gaps between the myelin sheaths along the axons, these are called the nodes of Ranvier. When an action potential is triggered at a Ranvier node, it will cause an ionic current that will flow rapidly through the myelin sheaths. The signal appears to leap between each node due to the depolarization of the myelin

sheath, which will in turn trigger an action potential of the next node. Myelin has low conductivity, which prevents the loss of electrical signals to surrounding tissue [11].
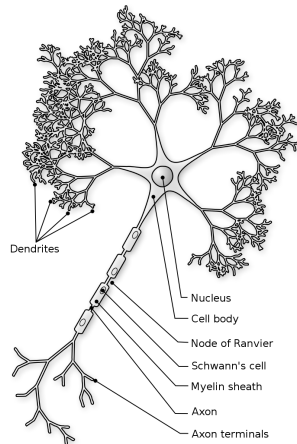
Figure 2.2: *Anatomy of the nerve cell. Used with permission from Wikimedia Commons. [12]*

The myelin concentration is highest in white matter (WM), where the myelin sheaths give its white appearance. The gray matter (GM) covers the surface of the brain, called cortex, and contains neural cell bodies, dendrites and unmyelinated axons, see Figure 2.3. The brain can be divided into two parts, the cerebrum and cerebellum. These are indicated in Figure 2.4. The ventricles, containing the cerebrospinal fluid (CSF), are located in the centre of the brain [11].
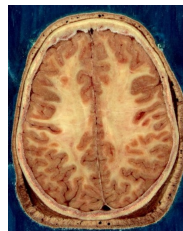
Figure 2.3: *White- and gray matter in the brain. Used with permission from Wikimedia Commons. [13]*

Figure 2.4: *Cerebrum and cerebellum, modified and used with permission from Wikimedia Commons. [14]*

The blood-brain barrier (BBB) refers to the capillary walls located in the CNS. The BBB regulates the exchange of ions and molecules between the blood and the CNS and it is far more regulated and selective compared to the other parts of the microvasculature system, due to its special endothelial cells. This barrier is vital in order to establish a proper neural function and to protect the nervous system from pathogens and toxins [15].

2.1.3 Pathogenesis

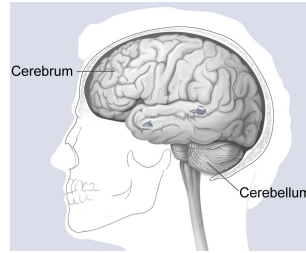MS is an autoimmune disease which causes an abnormal immune response against the body's own tissue, causing a degeneration of the myelin layer along the axons. This will slow down, distort or interrupt the nerve impulses propagating along the axon, causing the symptoms described earlier. The disease is called *Multiple Sclerosis* referring to the numerous scars, also called plaques or lesions, that are characteristic of the areas where the demyelination has occurred [16].
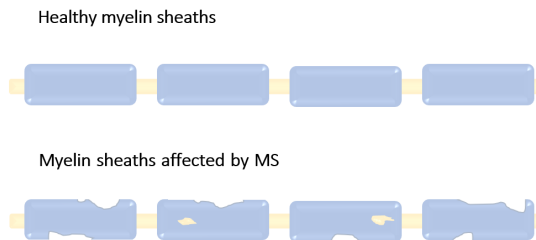
Figure 2.5: *Degeneration of myelin in MS*

The degeneration of myelin is caused by the loss of oligodendrocytes, which will complicate the maintenance of the myelin layer [7]. As the disease progresses, it does not only damage the myelin sheaths, with time it will also damage the axons, preventing the electrical signal to pass [1]. In the earlier stages of the disease the oligodendrocytes are capable to perform a remyelination of the axons, but this process does not last, causing the disease to progress in to the SPMS phase [7].

The BBB is thought to be disrupted during MS, resulting in an increased permeability, causing lymphocytes to migrate into the CNS. The migrated T- and B-cells undergo an autoimmune response against the myelin. The reason for this response is not fully known [15]. The autoimmune response will stimulate the B-cells to secrete immunoglobulins and multiply, and the T-cells start the degeneration of myelin [17]. The increasing number of B-cells are detected in the oligoclonal bands, which are used for diagnosis [15].

2.1.4   Progression of MS Lesions

It is widely agreed that the degree of disability in MS is correlated with axonal damage [2, 18–22]. The axonal damage is most active during the early stage of the lesion progress and the breakdown of the axons is more aggressive in the early years of the disease [2, 22]. A great correlation between myelin degeneration and axonal damage has been observed. The denuded axons appear to be more vulnerable to the toxic products produced by the macrophages [22], and myelin contribute with structural properties that maintain the cytoskeleton of the axon [2]. A correlation between axonal damage and numbers of macrophages and T-cells has been seen, suggesting that these also contribute to degeneration of the axons, either directly or due to toxic biproducts [2, 22]. During the acute phase, where degeneration of myelin and axons are most active, there is an increase in inflammation and oedema within the lesion [21]. The newly formed lesions often show a combination of demyelination, inflammation, oedema, axonal damage and early remyelination, since these processes occur dynamically, and not in any typical order [18]. Active lesions are often highly oedemic [21].

The nervous system is capable of remyelinating axons if there are a presence of oligodendrocytes, which reproduces the myelin sheaths, although with a shorter and thinner appearance [22]. The remyelination process is rapid and most efficient during the early MS stages. The remyelination appears most often at the rim of the lesion, but in some cases full repair is seen. These areas are referred to as *shadow plaques*. The remyelination reconstructs the structure of the axon and protects it from further destruction. The newly produced axon also restores the conductance over the axon, which improves the neurological function [23]. The lesions that do not manage to remyelinate may undergo necrosis. An expansion of the extracellular space is formed [18], causing extracellular free water to accumulate within the lesion [19].

2.1.5 Diagnosis

MS cannot be diagnosed by a single test. An international standard for the diagnosis is followed by the *McDonald Criteria* which are an approved diagnostic method that is used in 96% of the countries across the world [6]. The criteria can be summarized to that there has to be a dissemination in both time and space, i.e. there must have been inflammations in different locations that are typical for MS at at least two different time instances [5]. The criteria for dissemination in time can be fulfilled by an MRI scan, searching for active lesions which are enhanced by an injection of gadolinium contrast [24]. Typical MS lesions are cortical, infratentorial, juxtacortical, periventricular or located within the spinal cord. If there has only been one attack, a CSF examination should be performed, for example with protein electrophoresis which will detect the presence of oligoclonal bands, which has been proved to be a suitable prediction of a second attack [5].

2.1.6 Treatment and Therapy

At the time of writing there is no cure for MS, but disease-modifying therapies (DMTs) are used in most countries [6]. There are many kinds of DMTs, but all modulate or suppress the immune system. The agents can be given orally, by injection or by infusion with the aim to reduce the number of relapses and delay the progression of disability. The DMTs are unsuccessful for PPMS but have a beneficial impact on RRMS and SPMS. However, the treatment is complex, the disease is highly individual and is associated with many different side effects [25]. The treatment should be started as soon as possible to prevent axonal damage [2]. If the patient suffers from PPMS, a symptomatic treatment and physical therapy is used instead. At this stage it is not possible to restrain the development of the disease [25, 26].

2.2 Magnetic Resonance Imaging

Magnetic resonance imaging (MRI) is a technique used within the field of medical imaging. The technique uses the fundamental properties of the positively charged proton, i.e. the hydrogen nucleus, which is highly concentrated in fat and water. This is beneficial when identifying inflammation, since water is accumulated in those regions, making MRI a sensitive diagnostic technique [27].

All elementary particles inherit an intrinsic property called spin, which means that it rotates around its own axis. Due to the fact that it is a moving charge, it also means that it has a magnetic field surrounding it, and it is around the axis of this magnetic field that the proton rotates [27].

The patient is positioned inside the MR scanner where a strong magnetic field, B_0 is operating. The magnetic field will cause the protons to align with B_0, generating a net magnetization, M_0, that has the same direction as B_0. The precessional

frequency of the protons will adapt to B_0 according to the Larmor Equation 2.1, where γ is the gyromagnetic ratio of the hydrogen atom [27].

$$\omega_0 = \gamma B_0, \quad \text{where} \quad \gamma = 42,57\text{MHz/T} \tag{2.1}$$

The net magnetization of the body is much smaller compared with the external magnetic field, so it is not possible to measure the magnetization in this direction. For this reason, the signal will be measured in the transverse plane, which is accomplished by using a radio frequency (RF) pulse. The RF pulse oscillates with the given Larmor frequency and is generated by the transmit coil, acting as a constant magnetic field $B1$, on the effected protons. B_1 is perpendicular to B_0, and causes the protons and therefore also M_0 to turn into the transverse plane. The flip angle, α, is calculated according to Equation 2.2 [27].

$$\alpha = \gamma B_1 t_p \tag{2.2}$$

Often a flip angle of 90° is used, and it is accomplished by adjusting the duration of the pulse, t_p. The RF pulse will cause a coherent spin pattern. M_0 induces a current in the transmit coil where the voltage of the signal is measured. The signal decays exponentially, and M_0 aligns gradually with B_0 when the RF pulse is switched off. The relaxation times T1 and T2 are measured during the relaxation to the initial state. T1 is defined as the time required to reach 63% of M_0 and varies between different tissue types. Similarly, T2 is defined as the time required for the protons to dephase in the transverse plane [27].

Conventional contrast weighted images are generated by the use of different compositions of *pulse sequences*, which consist of the emitted RF-pulse and gradient pulses that are sent out with a specific pattern and timing. The two parameters *repetition time* (TR) and *echo time* (TE) control at which points in time the measurements appear, and adjustment of TR and TE makes it possible to acquire the desired tissue contrast [27].

In order to know the spatial position of the signal, gradients are added to the magnetic field. According to Equation 2.1, we know that a change in the static field B_0 will cause a change in frequency. The change in the gradient field in each position is known. The receiver is tuned into only detecting a specific frequency and it is therefore possible to determine where the signal has arisen [27].

2.2.1   Synthetic MRI

Synthetic MRI is a simulation method that is used to generate contrast weighted images based on an MR quantification scan. SyntheticMR uses a sequence that measures relaxation rates R1 and R2 and proton density (PD). The sequence uses multiple echoes which makes it possible to calculate T2 in each pixel since TE and TR are known. By repeating the sequence several times with varying delay times, it is also possible to calculate T1 in each pixel. This will result in a total of

eight images which can be transformed into R1, R2 and PD maps [28], see Figure 2.6.
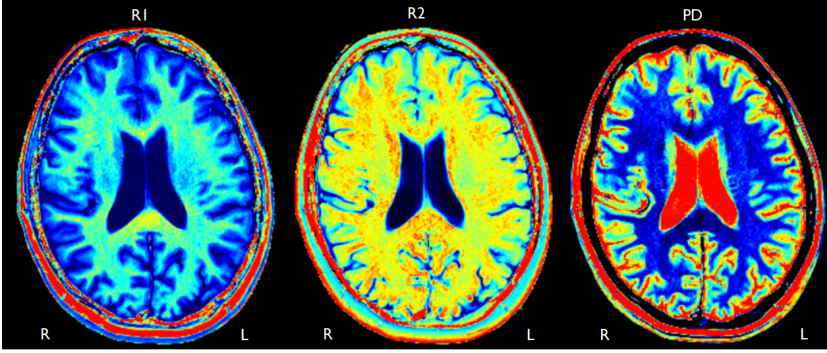

Figure 2.6: *Quantitative maps*

These maps chart the magnetic properties of the tissue and make it possible to synthesize the data into contrast weighted images such as T1W, T2W, PDW, T2W FLAIR and PSIR, appearing very similar to conventional images. Examples of synthetic images can be seen in Figure 2.7. Consequently, one could say that synthetic MRI is a form of translation where it is possible to translate the quantitative maps into contrast-weighted images [4].

Conventional MR has a disadvantage since the emitted signal intensity is affected by several scanner settings. The image appearance will for example be effected by inhomogeneities in the $B1$-field and sensitivities in the coils, which vary between different scanners but also between examinations, making it impossible to compare the intensities between images acquired at different time instances [28]. This disadvantage does not occur in synthetic MRI since the quantification has an absolute scale, which is independent of scanner settings and imperfections of the system [29, 30].

The synthetization is based on the signal equations, (Equation 2.3, 2.4 & 2.5) together with the result from the acquired parametric maps. By adjusting TR, TE and TI virtually it is possible to calculate a synthetic contrast weighting within each pixel. Equation 2.3 is used to create T1-, T2- and PD-weighted images, by adjustment of TR and TE [29].

$$S = PD(1 - e^{-R_1 TR})e^{-R_2 TE} \tag{2.3}$$

$$S_{PSIR} = PD(1 - 2e^{-R_1 TI} + e^{-R_1 TR})e^{-R_2 TE} \tag{2.4}$$

$$S_{FLAIR} = |S_{PSIR}| \quad \begin{cases} \text{where } TI \text{ is chosen so that} \\ (1 - 2e^{-R_1 TI} + e^{-R_1 TR}) = 0 \text{ for CSF} \end{cases} \tag{2.5}$$
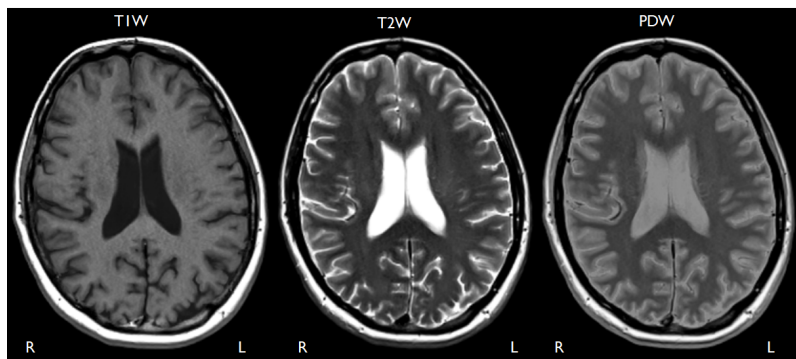
Figure 2.7: The synthetic weighted contrast images

SyMRI also generates different tissue maps, such as myelin, GM, WM and CSF. These maps are based on statistical studies on healthy subjects [31], an example of the tissue maps can be seen in Figure 2.8.
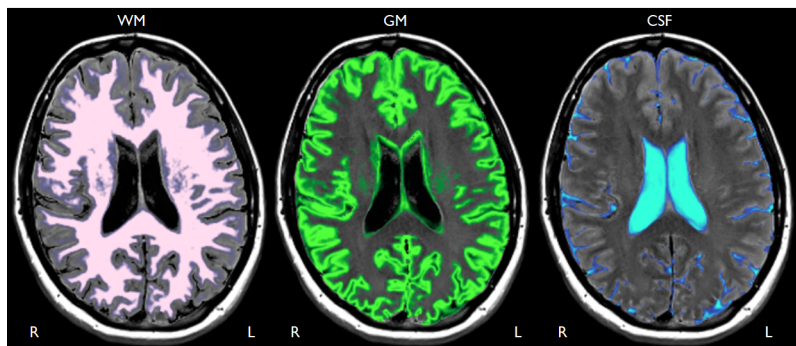

Figure 2.8: The tissue composition maps

2.2.2   Appearance of MS in MRI

As described in section 2.1.4, there is a change in tissue composition within the MS lesion, and these changes can be detected in an MR image. T2W FLAIR is commonly used to detect MS lesions due to their prominent appearance in this contrast weighting. Inflammation causes an accumulation of water which will generate a hyperintense appearance due to decreased R2 rate. One disadvantage with the T2W contrast weighted image is that it is incapable of describing disease activity. The hyperintense appearance can be a sign of inflammation, oedema or axonal loss, but it is not possible to differentiate these conditions [18, 20], resulting in a poor correlation between disability and T2W lesion load [22]. However, the T2W contrast is important to more easily fulfill the dissemination in space criteria for diagnosis [18].

Disease activity is estimated with the use of a contrast agent called gadolinium, which is a paramagnetic substance. An active lesion will accumulate the contrast agent, causing a hyperintense appearance in the T1W image due to the shortened T1 relaxation. This is an indication that there is a disruption of the BBB, and that the lesion belongs to an early inflammatory phase [20]. Unenhanced T1W lesions can be both hypointense and isointense, but are always hyperintense in T2W [18]. All lesions undergo this active phase, which lasts for 2-8 weeks before the damage of the BBB is repaired. The active lesions are a sign of myelin destruction [20], and long-time-active lesions run a greater risk of evolving to persistent *black holes* [18].

Unenhanced T1W lesions appear hypointense and are often referred to as black holes [2, 18]. The lower signal appears due to a widening of the extracellular space, that is created due to axonal loss and oedema. Many T1W lesions are isointense and are therefore not visible in the image. Most of the black holes show signs of irreversible tissue destruction and have a greater correlation of clinical disability than the T2W lesion load [18, 20]. Some black holes become permanent, others manage to disappear with time which is an indication of repair and remyelination. The black holes are more common in SPMS than in RRMS which may indicate that the remyelination mechanism is failing with the progression of the disease, causing increased disability [20].

The remyelination is a frequent process in MS and generates a hyperintense appearance in a T2W image. The signal is weaker compared to demyelinated lesions but brighter than normal appearing white matter. This is also true for the shadow plaques which are associated with full repair. The change in signal intensity can be explained by the newly produced myelin sheaths which are thinner than normal, causing a larger extracellular space. Similarly, this can be seen for T1W remyelinated lesions where the slightly expanded cellular space increases the T1 relaxation, generating a signal between the signals of white matter and demyelinated lesions [22].

Examples of three different lesion stages can be seen in Figure 2.9. The lesion located at the yellow arrow has a vague appearance in T2W FLAIR and PSIR, and is not visible in T1W, indicating an early stage of the progression phase. The lesion located at the orange arrow is visible in all images, the appearance in T1W indicates an increase of oedema and inflammation. The lesion located at the red arrow has a distinct appearance in T1W, indicating a black hole and severe axonal damage. The appearance is even more prominent in the PSIR image, and a dark area has appeared within the hyperintense lesion in T2W FLAIR. This indicates increased water content since the signal of the free water is suppressed by the inversion recovery.
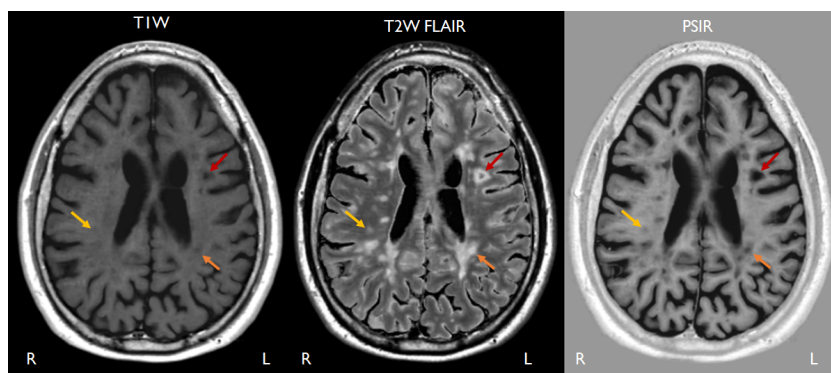

Figure 2.9: *An example of three lesions with different progression states*

3

Method

This chapter describes the method used in this study. The used data are described briefly, and a description of the manual segmentation is given. The implementation of the two aims is described including the approach to validate the results.

3.1 Study Participants

The data used for this study are divided in two separate groups. The first group consists of 4 healthy volunteers and the second group consists of 12 patients diagnosed with MS. The MS group consisted of eight females and four males, with a mean age of 36.82 ± 8.79 years. The healthy volunteers have a mean age of 39.33 ± 7.89 years with an equal distribution of men and women. During the implementation phase, two data sets of MS and two data sets of healthy volunteers were used. These data sets were not used in the validation phase.

3.2 Image Acquisition and Synthetisation

The data have been collected with a $3T$ Philips Medical Systems Achieva dStream scanner. The data have a slice thickness of $4.5mm$, slice gap of $0.5mm$ and an in-plane resolution of $0.6x0.6mm$ for the patients diagnosed with MS. For the volunteer data, there is a slice thickness of $4.0mm$, a slice gap of $1.0mm$ and an in-plane resolution of $0.48x0.48mm$. The data were collected by the QRAPMASTER sequence and post processed with SyMRI prototype 18Q3 (0.45.6). The different parameters used to synthesize the contrast-weighted images can be seen in Table 3.1.

Contrast	TR [ms]	TE [ms]	TI [ms]
T1W	500	10	–
T2W FLAIR	15000	100	3000
PSIR	6000	10	500

Table 3.1: *Parameters of the different contrast weightings*

The data is ethically approved and used with permission.

3.3 Manual Segmentation

The manual segmentation of the assumed MS lesions was performed by the author of this Master's Thesis, and is considered as ground truth for the validation. The segmentation was only performed for lesions located within WM, but in obvious cases, juxtacortical lesions were also included. A neuroradiologist at the Department of Radiology at Linköping University Hospital was consulted on how to segment lesions. However, the neuroradiologist has not verified the manual segmentation.

3.4 Implementation

The implementation was performed in Matlab 2017b (MathWorks, Natick, Massachusetts, USA) and the images were generated by SyMRI, including quantitative maps, synthetic contrast images and tissue composition maps.

3.5 Analysis of the MS Lesions

In order to understand the behaviour of the pathological voxels, they were studied in different parametric spaces. It was found that the lesion voxels were clustered within a specific area when imported to an R1-R2 space. This can be seen in Figure 3.1 where the green voxels are collected from a (whole) healthy brain, and the blue voxels are collected from the manually segmented lesions. As seen in Figure 3.1, the MS voxels have a specific distribution in the R1-R2 space, together with the typical locations for WM, GM and CSF [32]. This discovery was used to define the progression model and was also used in a minor part of the automatic segmentation algorithm.
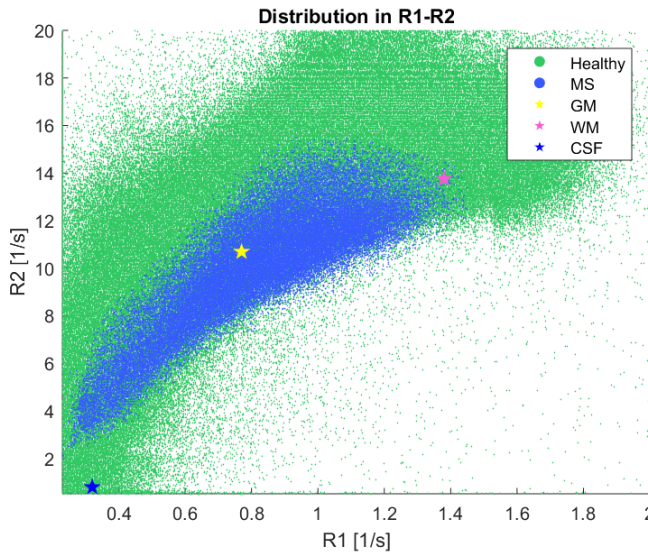
Figure 3.1: *The distribution between MS and healthy tissue*

3.6   Development of the Automatic Segmentation Algorithm

The algorithm operates slice wise and has been designed with the main purpose of eliminating areas that are non-pathological, taking advantage of the large information within the quantitative data. The structure of the algorithm can be seen in Figure 3.2 and is further explained below.
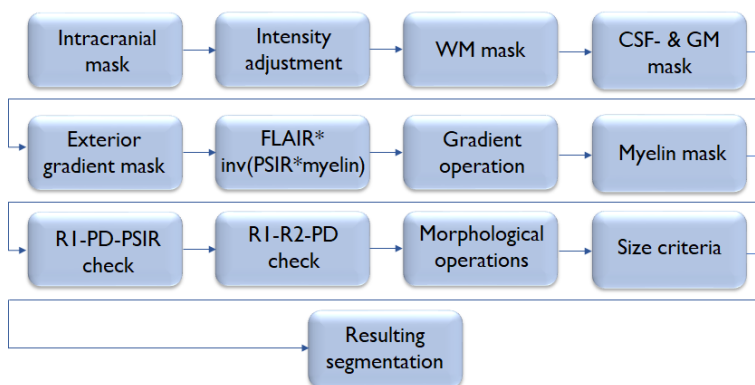

Figure 3.2: *The automatic segmentation algorithm*

3.6.1   Intracranial Mask and Intensity Adjustment

The development of the algorithm starts with the removal of the cranium which is done by using the intracranial mask available in the SyMRI software. An intensity adjustment is performed for the PSIR and FLAIR images since the values in these images are used later in the algorithm and need to be of similar magnitude.

3.6.2   WM Mask

A binary WM mask was created with the purpose of only keeping voxels consisting of white matter. However, lesions seldom contain any WM in SyMRI, due to the relaxation change caused by the degeneration of myelin and oedema. Therefore, an operation that covers the holes caused by lesions, ventricles or brain folds was added. The resulting mask can be seen in Figure 3.3.

Figure 3.3: The WM mask

3.6.3   CSF- & GM Mask

A CSF- and GM mask were used with the purpose of removing ventricles, brain folds, exterior fluids and cortex. It is important to create these two tissue types to one united mask since GM and CSF typically are connected, making the elimination more effective. However, all CSF- and GM voxels cannot be removed since lesions can mimic the appearance of GM tissue (non-myelinated) and CSF (severe tissue destruction).

The CSF mask is created in two separate steps since the periventricular lesions consist of a larger amount of water and therefore has to be treated separately. The separation was performed with a simple algorithm that differentiated the ventricles by finding a greater continuous area consisting of CSF located in the centre of the brain. A threshold of 75% was used for this area, removing all voxels having a larger CSF concentration than the threshold. For the exterior CSF a lower threshold was used, 20%, making it possible to remove brain folds of larger size. The edge of the intracranial mask was added with the purpose of connecting all exterior CSF.

A GM mask was thereafter created with a threshold of 70%. The three masks were merged together, as seen in Figure 3.4. However, small areas in the result-

ing mask were removed since these could be possible lesions. This mask is effective, since the added cranial edge reassures that the exterior CSF and connecting GM will be removed. However, the removal of smaller areas often results in that smaller brain folds remain after the operation.
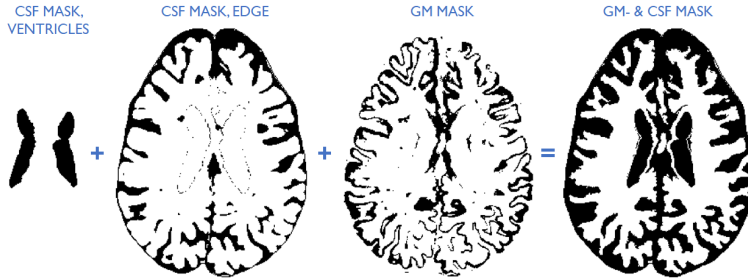

Figure 3.4: The different stages of the CSF- & GM mask

3.6.4   Exterior Gradient Mask

This step is performed to remove the outer parts of the cortex. This area is typically hyperintense in synthetic T2W FLAIR due to partial volume effects, but should not be confused with pathological tissue. The surroundings were modified to generate a large difference between the remaining tissue and the edges. A magnitude gradient, calculated in two directions was applied, generating large gradient at the edges, due to the great value difference. The resulting gradient image was translated into a binary image and thereafter used as a mask to remove the edges. The exterior gradient mask can be seen in figure 3.5
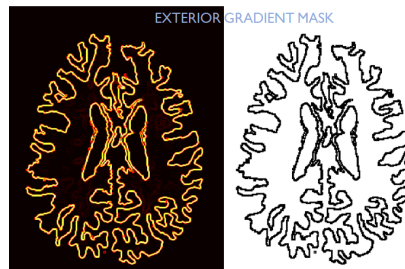

Figure 3.5: The exterior gradient mask

3.6.5   Multiplication of FLAIR, Inversed PSIR and Inversed Myelin

The purpose of this step was to enhance the lesions, making them more prominent compared to the surrounding nonpathological tissue. A multiplication of T2W FLAIR, PSIR and myelin was performed, where the PSIR image and the myelin map were inverted so that the lesions also appear hyperintense in these

images. The myelin tissue map was used since a decrease of myelin is an indicator of where the lesions are located. The result of this operation can be seen in Figure 3.6
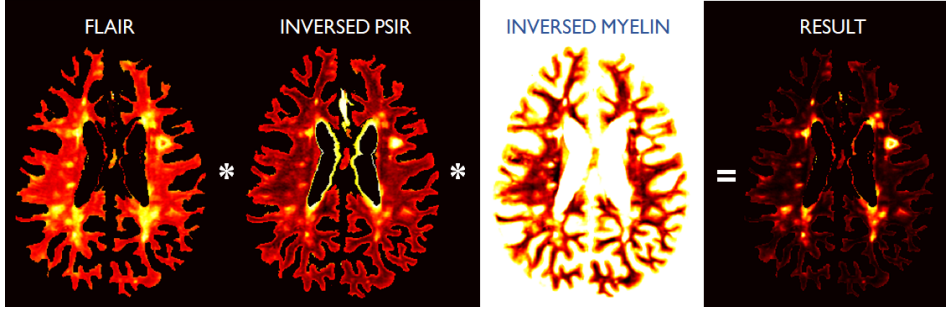

Figure 3.6: *A multiplication of T2W FLAIR, inversed PSIR and inversed myelin tissue map were used to enhance the lesions*

3.6.6 Gradient Operation

A gradient operation was performed to detect the lesion edges. This operation measures the gradient magnitude in two directions for each voxel. This is a good approach since lesions often are surrounded by WM, causing a prominent signal change because of their hyperintense appearance. The result of this operation can be seen in the first part of Figure 3.7. The gradient was thereafter binarized, resulting in the second part of the same figure. As can be seen, minor cortex objects remain in the lesion mask. Hence, an erosion was performed, excluding minor objects. By dilating this mask, and perform a multiplication with the first gradient mask, the remaining GM were removed, without shrinking the edges of the lesions. The final result is seen in the third part of Figure 3.7.
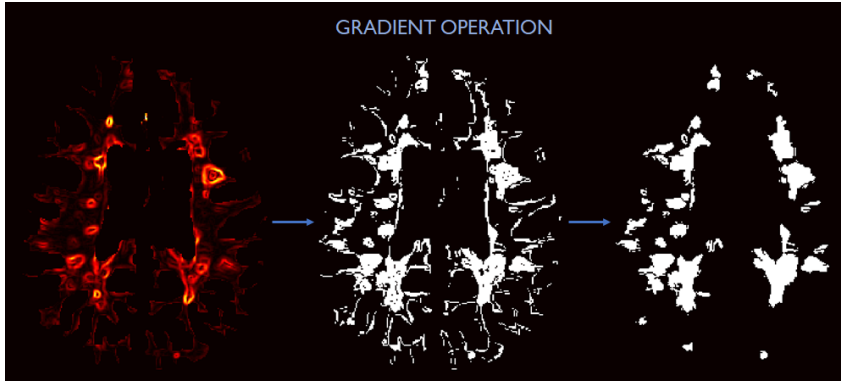
Figure 3.7: The gradient operation and resulting binary mask

3.6.7   Myelin Mask

This mask is used to take advantage of the pathogenesis of the lesions. Since the degeneration of myelin is one of the earliest processes, it is a good indicator of where the lesions are located. As before, the threshold has been chosen with care, so that early lesions do not vanish. The threshold was set so that voxels consisting of over 35% myelin are removed. The maximum concentration of myelin in SyMRI is 50%. The resulting mask can be seen in Figure 3.8.

Figure 3.8: The myelin mask

3.6.8   R1-R2-PSIR Check

In this step the analysis described in 3.5 was applied. After investigations it was found that a R1-R2-PSIR space was appropriate to differentiate healthy tissue from pathological, since the lesions always appear dark in a PSIR image. However, healthy tissue is also found within this distribution, and therefore unintentionally included. In order to determine if a voxel belongs to the space, an alpha shape was created, which is a shape that surrounds the voxels in the defined space. The inbuilt Matlab function *alphaShape*, was used with an alpha radius equal to 0.75. The resulting alpha shape and mask can be seen in Figure 3.9.
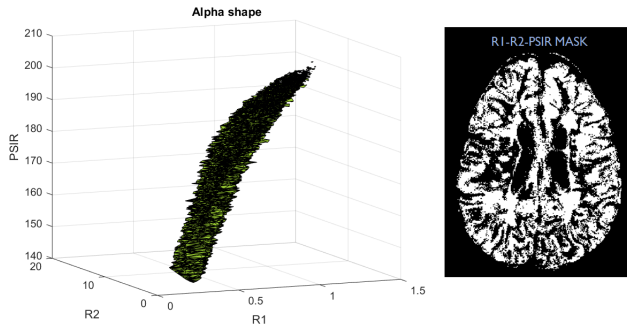
Figure 3.9: *Left: The alpha shape defining the MS cluster. Right: The resulting binary mask*

3.6.9   R1-R2-PD Check

A second parametric space was defined with the purpose of removing perivascular spaces. Perivascular voxels were segmented from two volunteer data sets and placed in a parametric space together with the segmented MS voxels. It was concluded that a R1-R2-PD space was most effective to differentiate the perivascular spaces from lesions. The implementation of the perivascular alpha shape was designed in the same way as described above. The resulting alpha shape and binary mask is seen in Figure 3.10
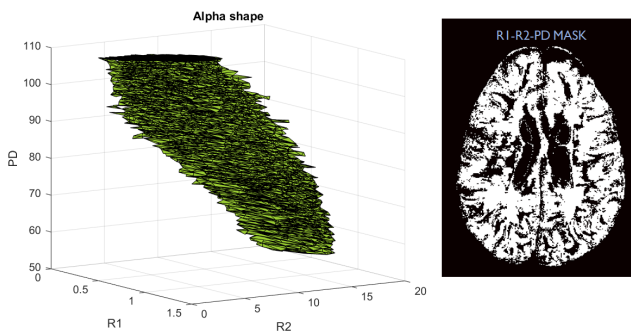

Figure 3.10: *Left: The alpha shape defining the space of perivascular spaces. Right: The resulting binary mask*

3.6.10   Morphological Operations and Size Criteria

Some morphological operations were performed in the last step of the algorithm which included the removal of spur pixels and to fill out minor holes in the already defined lesions. Thereafter smaller sized objects were removed. As described in 1.2.1, a lesion has a width of at least $3mm$ by definition. However, with the risk of removing too much pathological tissue in the earlier stages, a limit of $2.5mm$ was used in the algorithm, using the specific pixel width of the data set. The maximum distance within the detected lesion was calculated by applying the object pixels twice to the inbuilt matlab function *pdist2*, which calculates the pairwise distance between two sets of observations. If the size criteria was not fulfilled, the detected object was removed. Lastly, objects that had a geometry that did not include a 3x3 pixel shape were removed, since small slim objects often remains from brain folds while the lesions have a more expanded shape. The result can be seen in Figure 3.11.
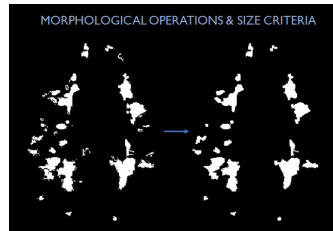

Figure 3.11: Morphological operation and fulfillment of size criteria

3.6.11   The Resulting Lesion Mask

The resulting lesion mask is applied to the image obtained in section 3.6.5 and translated into a colour scale. The final result of the automatic segmentation can be seen in Figure 3.12 where it is applied to the T2W FLAIR image.
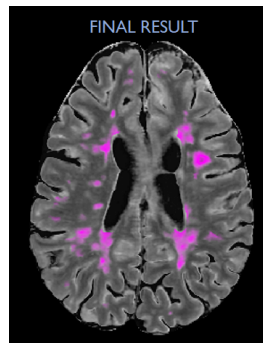

Figure 3.12: The final result of the segmentation

3.6.12   Summation of All Steps

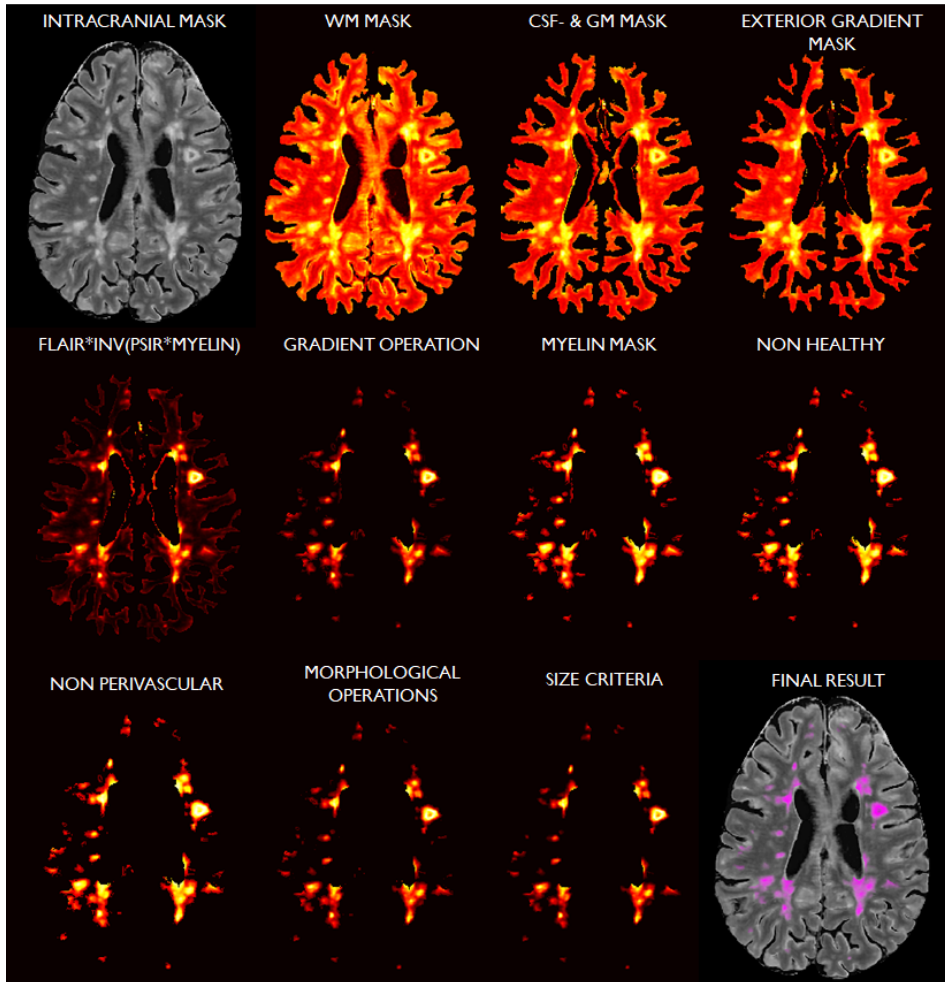The result from each step is summarized in Figure 3.13.

Figure 3.13: *The different steps of the automatic segmentation algorithm*

3.7 Development of the Progression Model

The structure of the progression model was mainly based on the discoveries described in 3.5. The idea was to mimic the pathological voxel "migration" through the R1-R2 space. As a prepossessing step, outliers were removed from the data to get a more robust model.

3.7.1 Calculation of the Progression Curve

Based on the MS cluster, a third-degree polynomial function $R2(R1)$ was estimated, using the curve fitting toolbox in Matlab. The third-degree polynomial was chosen since it mimicked the MS pattern most correctly, starting close to the CSF cluster position and ending close to the WM cluster position. The resulting equation can be seen in Equation 3.1 and the polynomial can be seen in Figure 3.14.

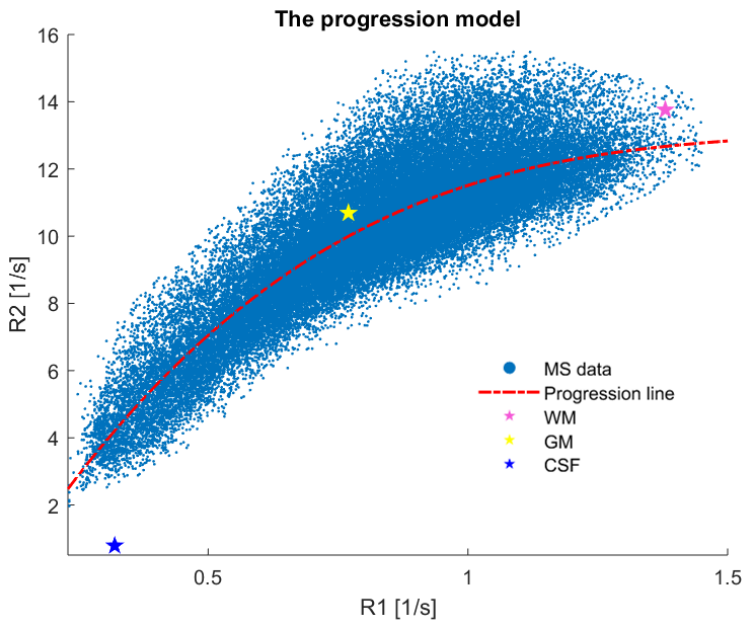$$R2(R1) = 3.259R1^3 - 16.05R1^2 + 27.29R1 - 2.989 \tag{3.1}$$

Figure 3.14: The calculation of the progression line $R2(R1)$

In the model it is assumed that a lesion travels from right to left by the progression line over time. The progression starts at the relaxation rates that are associated with healthy white matter. Demyelination and inflammation will cause the lesion to progress downwards the progression line, the further it goes, the more tissue destruction. A further progression is also associated with water accumulation due necrosis. However, a lesion could also wander in the opposite direction

with time, due to remyelination and healing of the tissue.

The progression line is associated with values between 0-100 that are evenly distributed throughout the line. A progression value of 0 is associated with healthy tissue and a progression value of 100 is associated with total tissue destruction. When performing the progression classification of an MS-voxel, the voxel is provided a progression value associated with the part of the progression line that is closest to the MS-voxel. Summarized, the progression model depends on both R1 and R2 and is limited to a value between 0-100, i.e. $Z(R1, R2) \in [0, 100]$.

3.7.2   The Resulting Progression Model

The progression model was applied to the manually segmented lesions, where the assigned progression value was translated into a colour scale, where red represents a further progression. An example of the this can be seen in Figure 3.15.
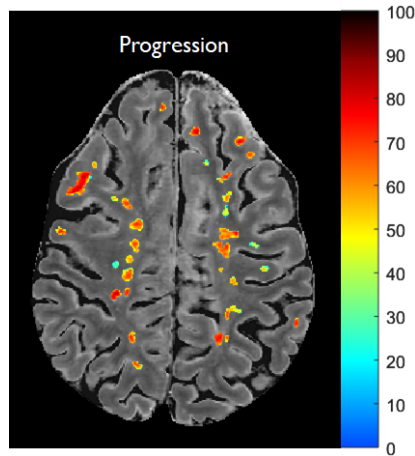

Figure 3.15: *The progression model*

3.8   Testing

In order to validate the results correctly, the testing data were not used during the implementation phase. The result from the automatic segmentation was compared with the manually segmented ground truth. The resulting progression model was tested on the manually segmented lesions and compared with the tissue maps and synthesized images in SyMRI.

3.9   Statistical Validation Tools

The results were validated based on two different methods. The first was to validate the result pixel wise, which indicates how well the overlap between the ground truth and the results were. These measures provide information of how well the algorithm segments the lesions and are here referred to as *sensitivity* and *precision*. The second method validates the total number of lesions, with the purpose of estimating how many lesions that were missed, and how many lesions that were falsely detected. A brief description of these statistical measures is seen below.

3.9.1   Statistical Measures of Performance

The statistical measures used for validation are dependent on the variables below.

- True positive (TP) - Lesion data that were classified correctly

- False positive (FP) - Non-lesion data that were classified incorrectly

- False negative (FN) - Lesion data that were classified incorrectly

If two lesions are merged together to one bigger lesion in the algorithm, this results as in two TP in the result. If only a part of the real lesion is segmented, this will be counted as one TP. The idea is to only look at the total number of lesions based on the ground truth, i.e. the size does not matter in this case.

The true positive rate (TPR) identifies the ratio between the real detected lesion and the total number of real lesions, see Equation 3.2. The positive predictive value (PPV) identifies the ratio between the real detected lesion and the total number automatically segmented lesions, see Equation 3.3 [33].

$$TPR = \frac{TP_{lesion}}{(TP_{lesion} + FN_{lesion})} \tag{3.2}$$

$$PPV = \frac{TP_{lesion}}{(TP_{lesion} + FP_{lesion})} \tag{3.3}$$

The above equations are also applied pixel wise, to avoid confusion, these are defined as sensitivity (Equation 3.4) and precision (Equation 3.5).

$$Sensitivity = \frac{TP_{pixel}}{(TP_{pixel} + FN_{pixel})} \tag{3.4}$$

$$Precision = \frac{TP_{pixel}}{(TP_{pixel} + FP_{pixel})} \tag{3.5}$$

3.9.2   Dice Similarity Coefficient

Dice similarity coefficient (DSC), which is a derivation of the Kappa statistics, was used to compare size and spatial location of the lesions between the manual and automatic segmentation. This measure is *only* used for the TP lesions, with the purpose of evaluate the overlap of the detected lesions. The formula for the DSC can be seen in Equation 3.6, where A is the manual segmentation, B is the automatic segmentation and n is the number of pixels [34]. Figure 3.16 illustrates the relationship of the intersection ∩.

$$DSC_{TP} = 2\frac{n\{A_{TP} \cap B_{TP}\}}{n\{A_{TP}\} + n\{B_{TP}\}} \tag{3.6}$$

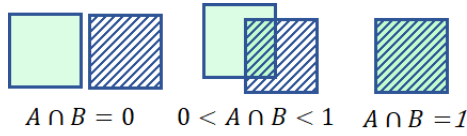$A \cap B = 0$ $0 < A \cap B < 1$ $A \cap B = 1$

Figure 3.16: *Definition of intersection*

The numerator measures the spatial overlap between the two segmentation types, and the denumerator measure the total amount of pixels in both segmentations. DSC equals to a value between 0 and 1, where 0 is no overlap and 1 is total overlap, a $DSC > 0.7$ is considered as a satisfactory result [34, 35]. DSC is more sensitive to location than size, which is a suitable approach since the manually segmented size of the lesion can differ vastly between radiologists [35]. An example of the location sensitivity can be seen in Figure 3.17.
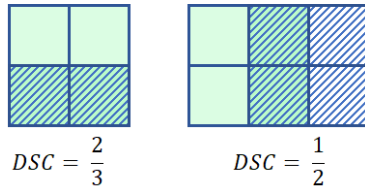

$DSC = \dfrac{2}{3}$ $DSC = \dfrac{1}{2}$

Figure 3.17: *An example of the DSC*

4

Results

The result of the two aims are presented in this chapter.

4.1 Results from the Automatic Segmentation

In this section are the results from the automatic segmentation presented. Statistical measures are presented in the Tables 4.1-4.6, where TPR and PPV is applied for each individual lesion and the sensitivity and precision is applied for each pixel in the image. The DSC is applied *only* to the TP lesions to get an idea how well the overlap is for the actual lesions.

Six tables are presented, one which includes all data sets (Table 4.1). Table 4.2-4.6 can be compared to see how the algorithm performs in the lower and upper part of the brain. For each statistical measure, mean-, max-, min and standard deviation values are given, and the tables are presented with some example images.

Whole brain	TPR	PPV	Sens	Prec	DSC
mean	0.75	0.38	0.62	0.23	0.56
min	0.00	0.00	0.00	0.00	0.00
max	1.00	1.00	1.00	0.86	0.97
σ	0.26	0.15	0.21	0.10	0.20

Table 4.1

4.1.1   Results from the Cerebellum and the Lower Part of the Cerebrum

Here are the results based on lesion location for the lower part of the brain, including images consisting of cerebellum in Table 4.2 and images containing the upper cerebellum together with the lower cerebrum in Table 4.3. Only seven data sets where used for the cerebellum since the remaining three did not contain any lesions in this area. The remaining tables is based on result from all ten data sets.

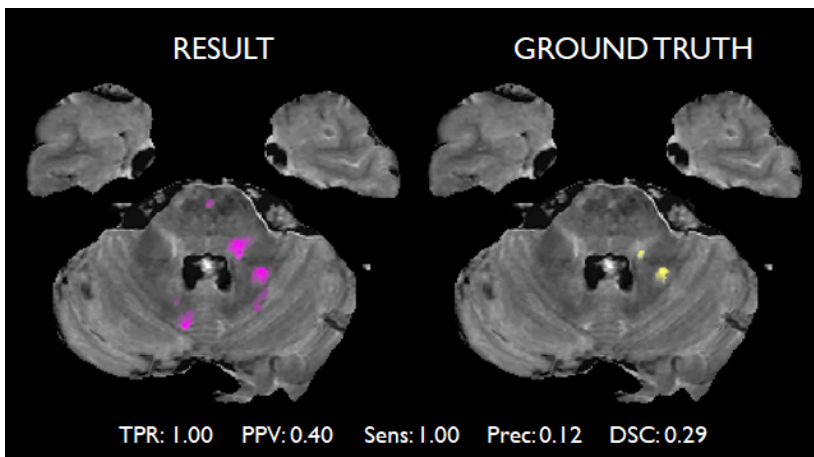| Cerebellum	TPR	PPV	Sens	Prec	DSC
mean	0.60	0.34	0.51	0.16	0.34
max	1.00	1.00	1.00	0.58	0.91
min	0.00	0.00	0.00	0.00	0.00
σ	0.40	0.23	0.35	0.13	0.25

Table 4.2

Figure 4.1: *Result from the cerebellum, a high sensitivity and TPR, but in this case are some FP lesions found, generating a lower precision and PPV.*

Cerebellum & cerebrum	TPR	PPV	Sens	Prec	DSC
mean	0.68	0.18	0.53	0.07	0.48
max	1.00	0.61	1.00	0.27	0.90
min	0.00	0.00	0.00	0.00	0.00
σ	0.29	0.10	0.23	0.05	0.23

Table 4.3

RESULT   GROUND TRUTH

TPR: 1.00   PPV: 0.10   Sens: 0.99   Prec: 0.04   DSC: 69
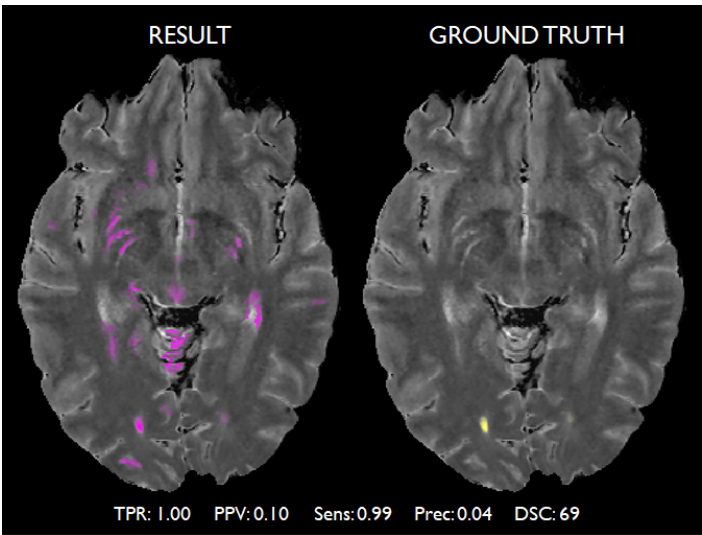
Figure 4.2: The upper cerebellum and the lower part of the cerebrum generates by far most FP lesions. GM has a much more complex structure in this area, causing the hyperintensities to be misinterpreted as lesions.

4.1.2   Results from the Cerebrum

Here are the results based on lesion location in the cerebrum. Table 4.4 shows the results from the lower part of the cerebrum and in Table 4.5 and 4.6 are the results from the middle versus the upper part of the cerebrum.

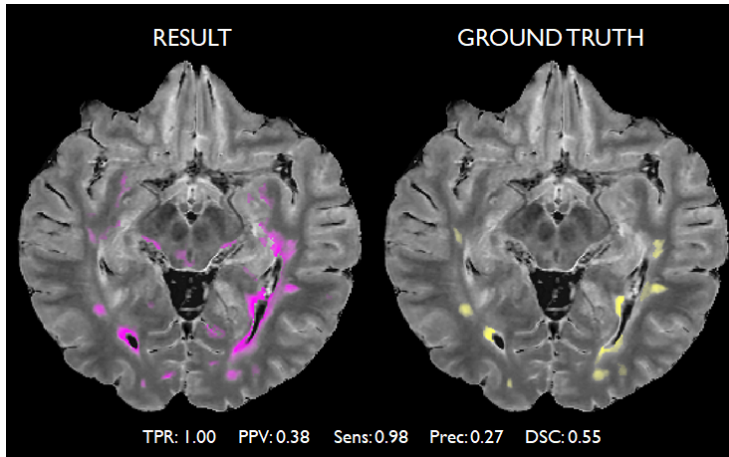| Lower cerebrum	TPR	PPV	Sens	Prec	DSC
mean	0.81	0.30	0.61	0.18	0.57
max	1.00	0.86	1.00	0.47	0.90
min	0.00	0.00	0.00	0.00	0.00
σ	0.28	0.13	0.26	0.10	0.25

Table 4.4

Figure 4.3: *The lower part of the cerebrum often generates many FP lesions, this is mainly due to the complex structure of GM.*
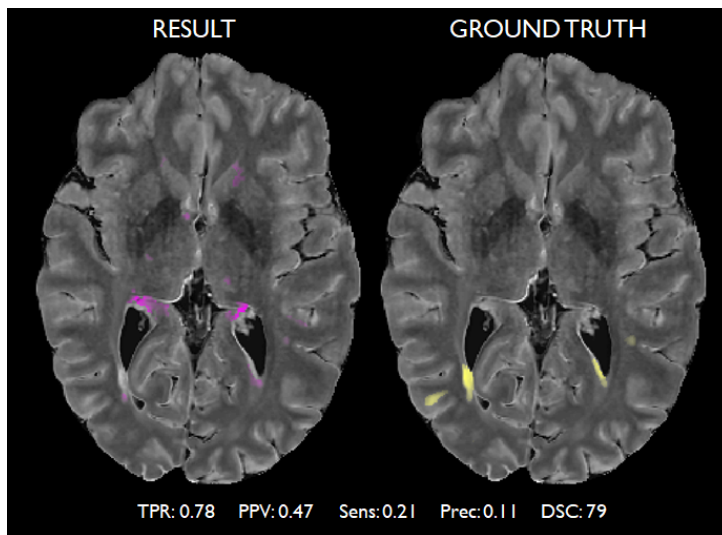

Figure 4.4: *The lower part of the cerebrum often generates many FP lesions, in this case, the partial volume around the ventricles affects the precision negatively.*

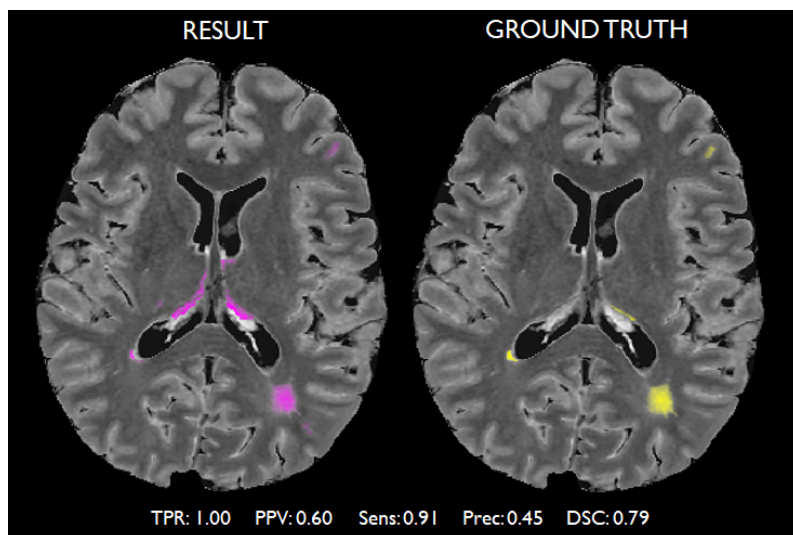| Middle cerebrum	TPR	PPV	Sens	Prec	DSC
mean	0.71	0.38	0.62	0.27	0.60
max	1.00	0.94	1.00	0.70	0.97
min	0.00	0.00	0.00	0.00	0.00
σ	0.27	0.20	0.27	0.17	0.26

Table 4.5

Figure 4.5: *The middle part of the cerebrum. The sensitivity and TPR indicates good results, but the precision and PPV indicates that quite many FP are found. In this case, the partial volume around the ventricles affects the precision negatively. The DSC for the TP lesions indicates a satisfactory result.*
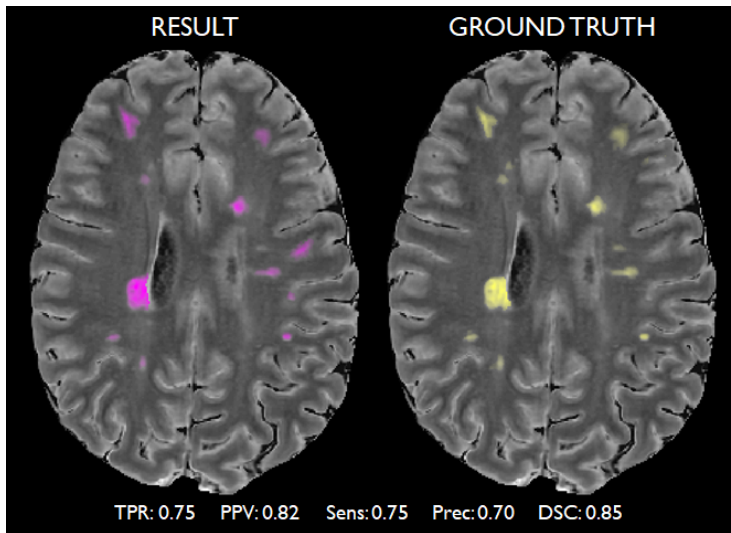
Figure 4.6: *The middle part of the cerebrum. A relatively good result over-all, only a few lesions have been missed out and the DSC for the TP lesions indicates a satisfactory result.*
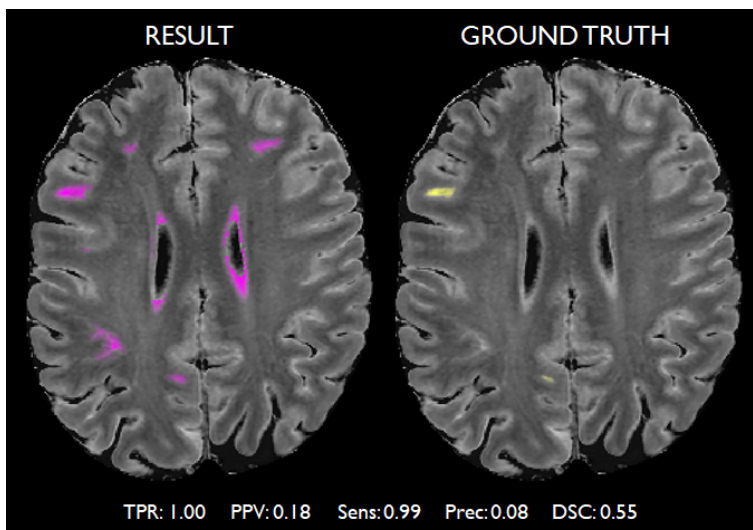

Figure 4.7: *The middle part of the cerebrum, where the main issue for the segmentation is the partial volume due to the large slice thickness, both around the ventricles and shallow brain folds. This generates a severely low PPV and precision.*

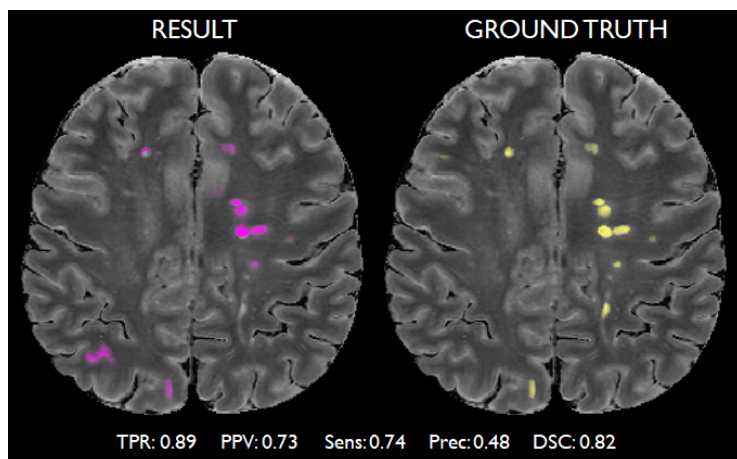| Upper cerebrum	TPR	PPV	Sens	Prec	DSC
mean	0.71	0.47	0.61	0.29	0.57
max	1.00	1.00	1.00	0.84	0.95
min	0.00	0.00	0.00	0.00	0.00
σ	0.31	0.22	0.26	0.14	0.24

Table 4.6

Figure 4.8: *Upper part of the cerebrum where the majority of lesions are found. Some brain folds, (lower part of the image) are mistaken as lesions.*
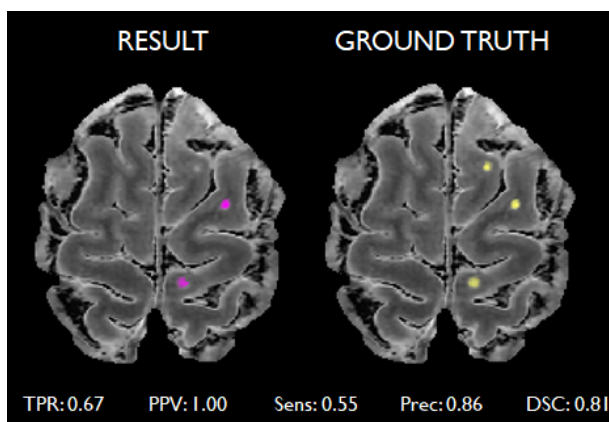

Figure 4.9: *The upper part of the cerebrum, 2 of 3 lesions where found. The DSC for the TP lesions indicates a satisfactory result. Since no FP lesions where found, the precision and PPV is high.*

4.2   Results of the Progression Model

The result from the progression model is presented in Figure 4.11, 4.14, 4.17, 4.20 and 4.23. Each one of these figures are accompanied with figures generated by SyMRI for comparison. The T1W is added with the purpose of differentiate tissue destruction via the black holes and T2W FLAIR is used for an intensity comparison. The myelin map is added to see how far gone the demyelination is and the CSF map is added with the purpose of finding water accumulations. Lastly, the NON map is added which resembles pixels that have not been classified by SyMRI. This map is added since lesion areas frequently are classified as NON, since these areas do not resemble healthy tissue. In Figure 4.10, the relationship between the progression value and the mentioned parameters can be seen.
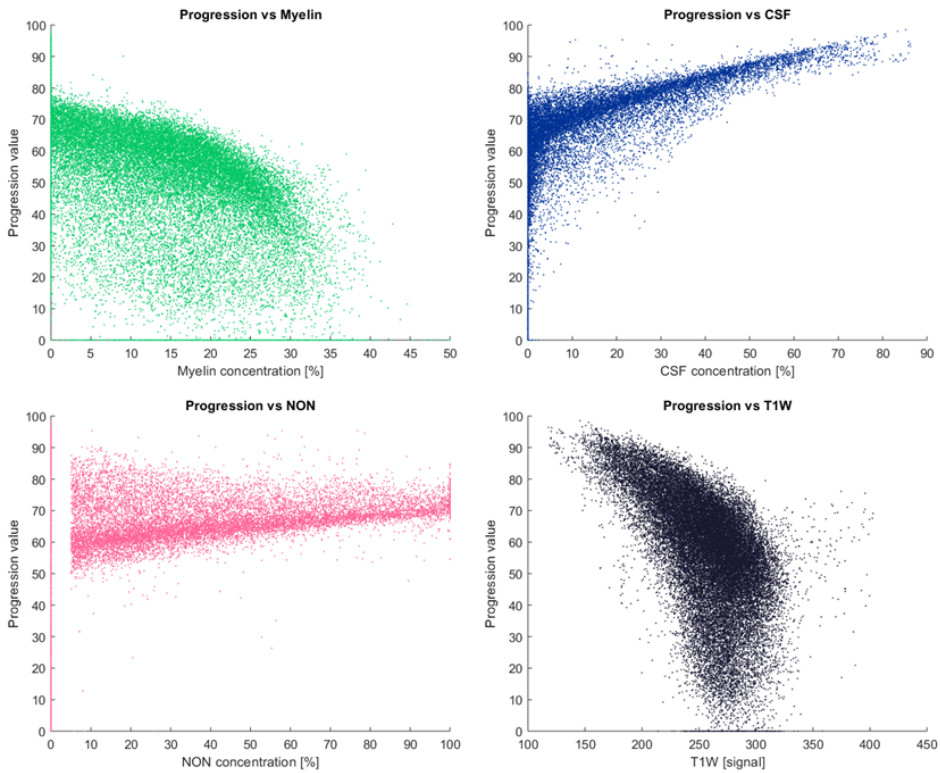

Figure 4.10: *The relation between the progression value and myelin-, CSF-, and NON-concentration and the synthesized T1W signal. This proves that the progression value correlates with the tissue changes seen during lesion progression.*
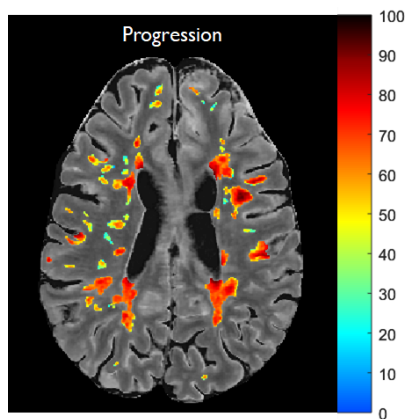
Result Example 1

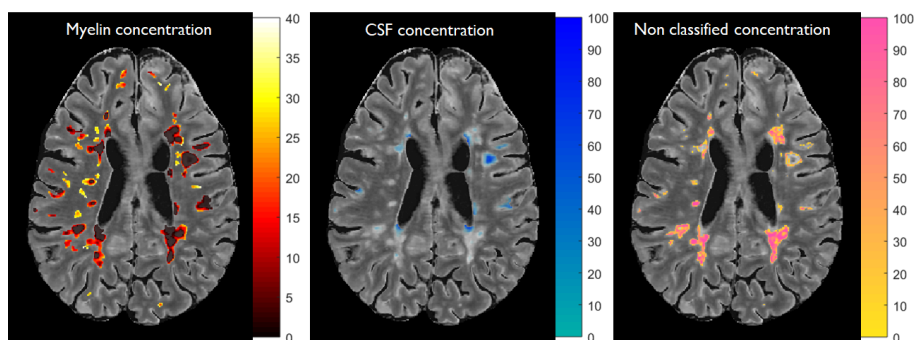*Figure 4.11:* *Final result of the progression model*

Figure 4.12: *Tissue concentrations generated by SyMRI*

Figure 4.13: *T2W FLAIR and T1W generated by SyMRI*

Result Example 2

Figure 4.14: *Final result of the progression model*

Figure 4.15: *Tissue concentrations generated by SyMRI*

Figure 4.16: *T2W FLAIR and T1W generated by SyMRI*

Result Example 3

Figure 4.17: Final result of the progression model

Figure 4.18: Tissue concentrations generated by SyMRI

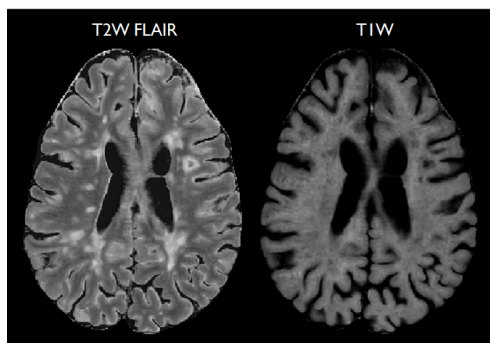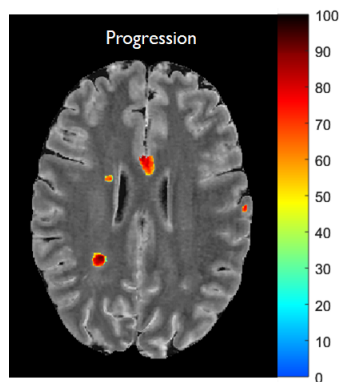*Figure 4.19:* T2W FLAIR and T1W generated by SyMRI

Result Example 4

Figure 4.20: *Final result of the progression model*

Figure 4.21: *Tissue concentrations generated by SyMRI*

Figure 4.22: *T2W FLAIR and T1W generated by SyMRI*

Result Example 5
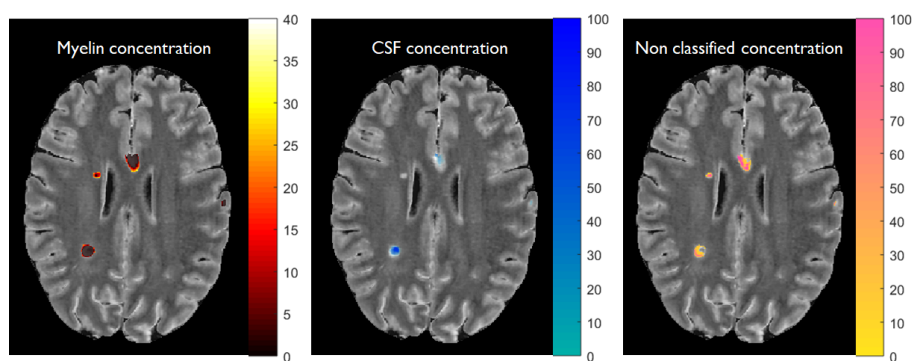

Figure 4.23: Final result of the progression model

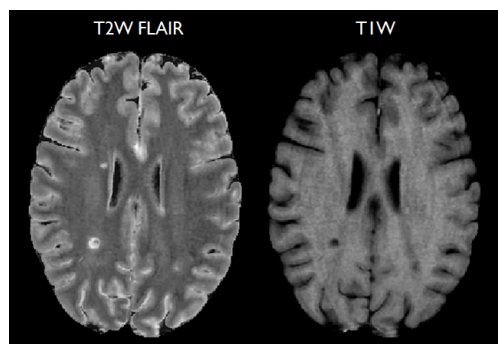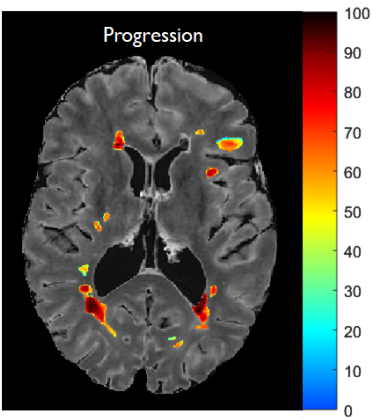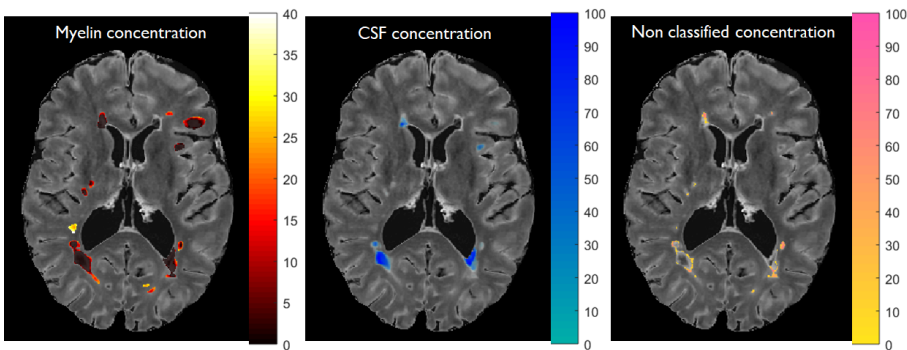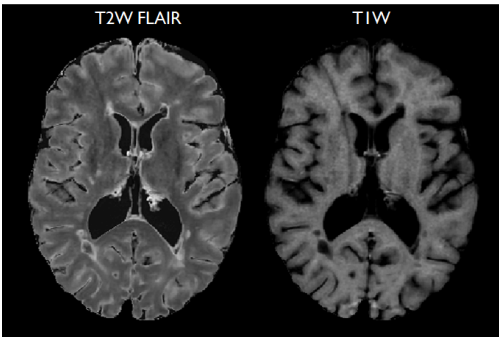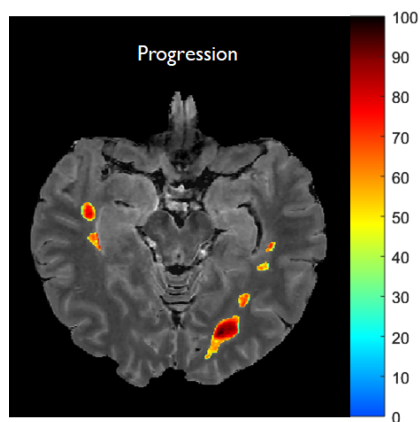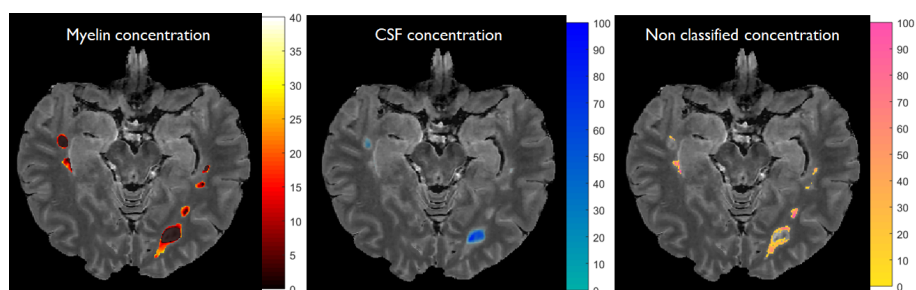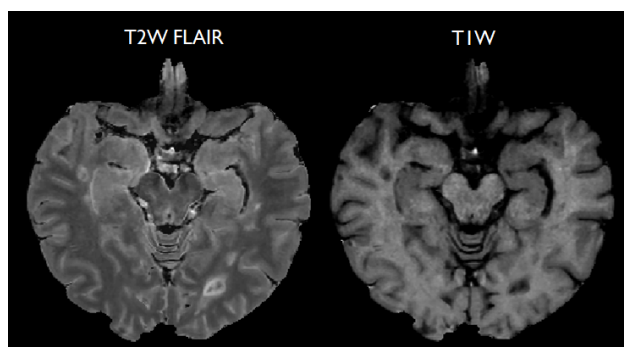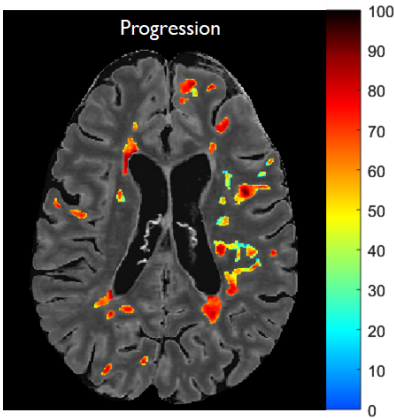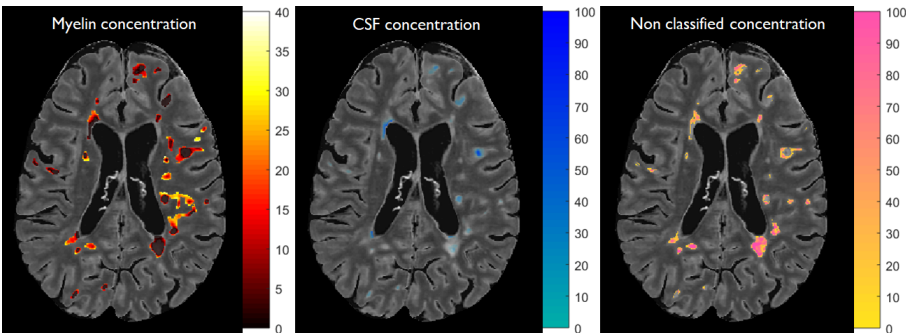*Figure 4.24: Tissue concentrations generated by SyMRI*
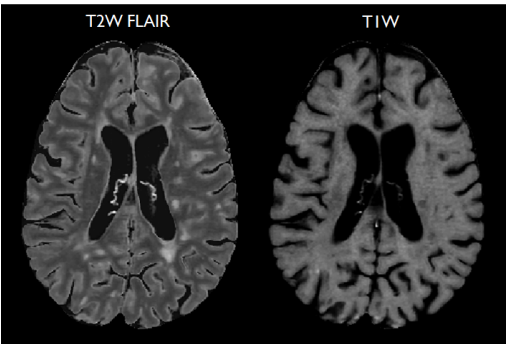
Figure 4.25: T2W FLAIR and T1W generated by SyMRI

5

Discussion

This chapter contains a discussion based on the results seen in chapter 4. The results from the automatic segmentation algorithm and the results from the progression model are discussed separately.

5.1 Automatic Segmentation Algorithm

From the result in section 4.1 it can be seen that the automatic segmentation algorithm is fairly sensitive, but not precise, meaning that most of the lesions are found, but many FP lesions are detected. It can also be seen that the algorithm generally performs better in the cerebrum. The poor performance can partly be explained by the lack of data, the algorithm was implemented using only two data sets, which is too few to create a robust solution.

Table 4.1 indicates that approximately 75% of the true lesions where found and that approximately 38% of the detected lesions are correct. This is not a satisfying result, since a very large number of FP lesions are detected. However, the algorithm was designed to be sensitive, since a radiologist needs support to find the vague lesions, the prominent are easily found. Some of the FP lesions can be ruled out by the author, but some of these could be TP lesions, but a radiologist would need to confirm this.

When observing Tables 4.2-4.6 it can be concluded that the algorithm performs differently depending on brain location. Best result was seen in the middle and upper part of the cerebrum where approximately 70% of the true lesions were found. The upper cerebrum generates the largest PPV and precision meaning that fewer FP lesions are found here. However, approximately 50% of the segmented lesions are FP, so the result is not satisfactory. Lowest precision is seen in

the images of the combined cerebrum and cerebellum, where an extreme amount of FP lesions are found. The best result of the DSC is seen in the cerebrum with a mean of approximately 0.60. This indicates a fairly good overlap, having in mind that a satisfactory DSC is greater than 0.70, as mentioned in section 3.9.2. However, it is important to remember that this result only regard the TP lesions, the result would have been lower if the FP lesions were included.

It has previously been reported that synthetic T2W FLAIR suffers from hyperintensity artifacts which are not present in conventional images [36] [37]. The hyperintensity artifact occur in synthetic images due to partial volume, where the signal from both CSF and parenchyma is detected in each voxel. This is not the case for conventional FLAIR images, where the signal from CSF is fully suppressed. It is probable that the automatic segmentation algorithm would perform better if this artifact did not exist, since the algorithm is designed to detect T2W FLAIR hyperintensities.

The large slice thickness of $4.5mm$ causes problems, since it causes shallow ventricles and brain folds to appear hyperintense in the synthetic T2W FLAIR, due to the partial volume effects described above. An example of this can be seen in Figure 5.1.
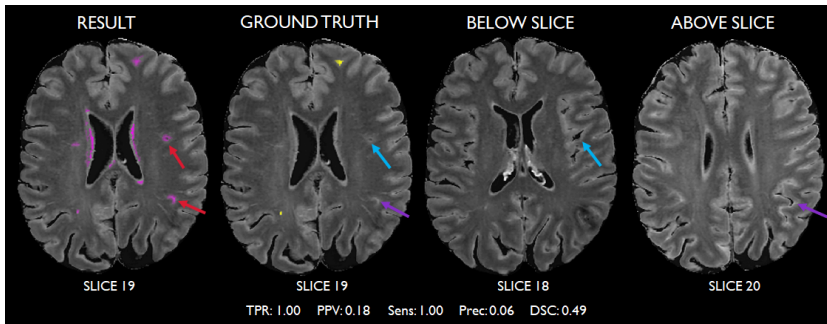
Figure 5.1: *The precision and PPV is low due to the detection of shallow brain folds, appearing as hyperintense areas in the synthetic T2FLAIR image. These FP lesions (red arrows) are pointed out at the adjacent slices (blue and purple arrow). Also note the partial volume around the ventricles which also affects the result.*

The large slice thickness causes an averaging of the signal creating a partial volume effect, especially around the ventricles and brain folds. The signal is therefore interpreted as tissue with an increased water concentration, which is very similar to the tissue composition of a lesion. This caused the algorithm to mistakenly identify these areas as pathological, which effected the results negatively. After studying several images over the cerebrum, it was found that the FP lesions mainly occurred due to this problem. According to Rovira et al. a slice thickness of $3mm$ is recommended [24], this should be considered in future studies.

The algorithm performs poorly in slices that include both the cerebrum and cerebellum. GM has a more complex structure here, interacting with WM to a larger extent. This causes the GM mask in the algorithm to be less "connected", and due to this, parts of the GM are not removed. Comparing this to the wide areas of WM in the cerebrum, it is easy to understand the difficulties of detecting lesions within this area. Furthermore, this part of the brain was by far the most complex part to analyze during manual segmentation, so it is not surprising that a poor result is seen here.

A major drawback is the small amount of data used in this study. The algorithm was developed on two data sets, and the development was mainly performed within the middle of the cerebrum. This is reflected in the result, since the algorithm were unintentionally designed to perform better in this part of the brain. Furthermore, during implementation, data sets with a high lesion load were used. This can partly explain the low precision, since the algorithm was designed to detect vague lesions. When the algorithm is applied to a brain with a low lesion load, it is too sensitive and detects nonpathological tissue.

Lastly, it should be mentioned that the results from this implementation can be questioned, since the ground truth has been stated by the author of this report. It is probable that some lesions have been missed, but also possible that healthy tissue has been misclassified. This could affect the results, either good or badly. The results could also be biased, since the author has created the algorithm based on her opinion of lesion appearance. It would have been desirable to have a neuroradiologist who performed the manual segmentation.

5.2   Progression Model

Unlike the automatic segmentation algorithm, the progression model is not compared to a binary ground truth and cannot be validated based on the statistical measures used above. However, the result can be compared to the synthesized MR images and the tissue maps generated from SyMRI and the theory summarized in 2.1.4 and 2.2.2.

The progression model indicates a fairly good correlation with the quantitative myelin concentration. Where total myelin degeneration is seen, the progression model confirms a further progression. When studying the myelin graph in Figure 4.10, it can be seen that a higher concentration of myelin correlates with a minor progression value. In this graph it can also be seen that complete myelin destruction appears for progression values larger than approximately 75.

When studying the CSF graph in Figure 4.10, it can be seen that the CSF concentration is linearly increasing for larger progression values, this is also seen in the CSF images where a further progression correlates with a larger accumula-

tion of water. This agrees with theory, since high water concentration indicates a widening of the extracellular space due to tissue destruction. From this graph it can also be concluded that lesions with a minor progression value does not contain any water. However, the CSF map represent *free water*, meaning that parenchymal water due to inflammation and oedema is excluded. This tissue is typically classified as NON instead, since this tissue composition does not appear in a healthy brain. The lesion areas classified as NON, appear to have a decrease in R2 rate compared with areas with a lower progression values, which indicates oedema. So even if the CSF concentration is classified as 0 in these areas, they most likely consist of parenchymal water to some extent.

Lesions classified with a larger progression value are hypointense in the T1W image, which is a promising result since the black holes are associated with tissue destruction. It can also be seen that pixels classified with a progression value smaller than approximately 70 are isointense in the T1W image, which indicates just a small (or no) tissue destruction. This relationship can also be seen in the T1W graph in Figure 4.10.

Studying the T2W FLAIR weighted images, it can be seen that hypointense areas correspond to a larger progression value. This is a sign of water accumulation and severe tissue destruction since the signal is suppressed.

Based on this, it can be concluded that the progression model could be a useful tool clinically, since it summarizes the information seen in the T1W- and T2W FLAIR images and the CSF- and myelin maps. A great advantage is that the model is based on quantitative data, making it possible to study the progression over time for an individual patient.

It is possible that this type of solution could be used to give an indication of when to change medication or to better understand the disease progression of the patient. Furthermore, it is possible that the model could substitute the use of gadolinium in the diagnostic phase, if it can be proven that lesions with different progression states could indicate separate attacks.

6

Conclusion

The purpose of this master's thesis was to develop an automatic segmentation algorithm and a progression model for white matter MS lesions. The conclusions from these two aims are presented below.

Create an algorithm that performs an automatic segmentation of possible multiple sclerosis lesions.

An automatic segmentation algorithm was implemented with the purpose of segmenting possible multiple sclerosis lesions. The results indicate a relatively high sensitivity, detecting approximately 70 – 80% of the cerebrum lesions, but generally with a low precision. The low precision was especially seen in the combined cerebellum and cerebrum, where the gray matter has a more complex structure. The large number of FP lesions occurs mainly due to the large slice thickness of the data, making shallow brain folds and ventricles to mimic the characteristics of multiple sclerosis lesions. One major disadvantage was the lack of appropriate data, the development of the automatic segmentation algorithm was developed on two data sets with high lesion load, more data would have been desirable.

Examine whether any characteristics of multiple sclerosis lesions can be found in the quantitative MR data, and propose a model that classifies these lesions based on their progression.

It was found that the multiple sclerosis lesions are located in an explicit area within the R1-R2 space and that both these values are decreased with increased tissue destruction. The progression model was implemented based on these insights, estimating a third-degree polynomial which mimicked the change in relaxation rates. The resulting model was thereafter assigned a progression value between 0-100 which was evenly distributed over the estimated polynomial.

The progression model showed promising results when compared with synthetic and quantitative data and could be interesting to develop further. It is possible that this type of model could be useful when monitoring patients with MS, assisting the neuroradiologist with quantitative information regarding the lesion states. It is possible that this could ease decisions regarding medication, but also to eliminate the use of gadolinium during diagnosis, if it can be proven that it can fulfill the dissemination in time McDonald criteria.

7

Future Work

In this chapter are some thoughts and ideas presented of how the two aims could be developed further in the future.

7.1 Automatic Segmentation Algorithm

First of all, it would be desirable to increase the number of subjects during the implementation phase, which would increase the possibilities of a more robust algorithm. It is also possible that a more robust automatic segmentation algorithm could be developed if the algorithm were adapted by lesion location in the brain. The result of this report showed a better result in the cerebrum, and it should be possible to adapt the algorithm to perform better in the cerebellum as well. The segmentation should also preferably be divided in lesion types, so that the different types of lesions (i.e. juxtacortical, periventricular etc.) can be treated separately. This would increase the sensitivity of the algorithm. Future work should also include cortical lesions which can be detected in the double inversion recovery (DIR) weighting [24].

7.2 Progression Model

The progression model indicates a promising result but could be developed further to be more useful clinically. A suggestion is to investigate how the progression value change over time for each individual lesion. By finding the maximal progression pace, it is possible that a progression model could fulfill the dissemination in time criteria during diagnosis. If a patient has both far progressed and non-far progressed lesions, it could be a sign of two separate attacks. Hence, it would be possible to get an earlier diagnosis, without the negative effects of the

gadolinium contrast. Furthermore, it could be investigated how different medications affect the lesion progression, it is possible that this type of tool could ease the monitoring of the patient. Lastly, it could be interesting to compare the progression distribution between the different MS types.

Bibliography

[1] Goldenberg MM. Multiple Sclerosis Review. P T. 2012;37(3):175–184. Cited on pages 1 and 8.

[2] Kuhlmann T, Lingfeld G, Bitsch A, Schuchardt J, Brück W. Acute axonal damage in multiple sclerosis is most extensive in early disease stages and decreases over time. Brain. 2002;125(10):2202–2212. Cited on pages 1, 9, 10, and 14.

[3] Brady AP. Error and discrepancy in radiology: inevitable or avoidable? Insights Imaging. 2017;8(1):171–182. Cited on page 1.

[4] Warntjes JB, Leinhard OD, West J, Lundberg P. Rapid Magnetic Resonance Quantification on the Brain: Optimization for Clinical Usage. Magn Reson Med. 2008;60(2):320–329. Cited on pages 3 and 12.

[5] Thompson AJ, Banwell BL, Barkhof F, Carroll WM, Coetzee T, Comi G, et al. Diagnosis of multiple sclerosis: 2017 revisions of the McDonald criteria. Lancet Neurol. 2018;17(2):162–173. Cited on pages 4 and 10.

[6] Multiple Sclerosis International Federation. Atlas of MS 2013, mapping the multiple sclerosis over the world; 2013. Cited on pages 5 and 10.

[7] Compston A, Coles A. Multiple Sclerosis. Lancet. 2008;372(9648):1502–1517. Cited on pages 5 and 8.

[8] Wingerchuk DM. Smoking: effects on multiple sclerosis susceptibility and disease progression. Ther Adv Neurol Disord. 2012;5(1):13–22. Cited on page 5.

[9] Nakahara J, Maeda M, Aiso S, Suzuki N. Current Concepts in Multiple Sclerosis: Autoimmunity Versus Oligodendrogliopathy. Clin Rev Allergy Immunol. 2012;42(1):26–34. Cited on page 6.

[10] Høglund RA, Maghazachi AA. Multiple sclerosis and the role of immune cells. World J Exp Med. 2014;4(3):27–37. Cited on page 6.

[11] Tortora G, Derrickson B. Principles of Anatomy & Physiology. 13th ed. Johan Wiley & Sons; 2011. Cited on page 7.

[12] Rougier N. Biological neuron schema; 2007. Wikimedia Commons. Available from: `https://commons.wikimedia.org/wiki/Neuron#` `/media/File:Neuron-figure.svg`. Cited on page 7.

[13] National Library of Medicine. Visible Human head slice; 1995. Wikimedia Commons. Available from: `https://commons.wikimedia.org/wiki/` `File:Visible_Human_head_slice.jpg`. Cited on page 7.

[14] Hoofring A. Major Parts of the Brain; 2001. Wikimedia Commons. Available from: `https://commons.wikimedia.org/wiki/File:Major_` `parts_of_the_brain.jpg`. Cited on page 8.

[15] Daneman R, Prat A. The Blood–Brain Barrier. Cold Spring Harb Perspect Biol. 2015;7(1):a020412. Cited on pages 8 and 9.

[16] Zawada WM, Campanella JJ. Multiple sclerosis. Magill's Medical Guide. Salem Press (Online Edition); 2013. Cited on page 8.

[17] Walsch CJ. Immune response to bacterial infections. Encyclopedia of Health. Salem Press (Online Edition); 2014. Cited on page 9.

[18] Sahraian MA, Radue EW, Haller S, Kappos L. Black holes in multiple sclerosis: definition, evolution, and clinical correlations. Acta Neurol Scand. 2010;122(1):1–8. Cited on pages 9 and 14.

[19] Loevner LA, Grossman RI, McGowan JC, Ramer KN, Cohen JA. Characterization of Multiple Sclerosis Plaques with T1-Weighted MR and Quantitative Magnetization Transfer. AJNR Am J Neuroradiol. 1995;16(7):1473–1479. Cited on page 9.

[20] Barkhof F, van Walderveen M. Characterization of tissue damage in multiple sclerosis by nuclear magnetic resonance. Philos Trans R Soc Lond B Biol Sci. 1999;354(1390):1675–1686. Cited on page 14.

[21] Giacomini PS, Levesque IR, Ribeiro L, Narayanan S, Francis SJ, Pike GB, et al. Measuring Demyelination and Remyelination in Acute Multiple Sclerosis Lesion Voxels. Arch Neurol. 2009;66(3):375–381. Cited on page 9.

[22] Barkhof F, Bruck W, De Groot CJ, Bergers E, Hulshof S, Geurts J, et al. Remyelinated lesions in multiple sclerosis: magnetic resonance image appearance. Arch Neurol. 2003;60(8):1073–1081. Cited on pages 9 and 14.

[23] Patani R, Balaratnam M, Vora A, Reynolds R. Remyelination can be extensive in multiple sclerosis despite a long disease course. Neuropathol Appl Neurobiol. 2007;33(3):277–287. Cited on page 9.

[24] Rovira A, Wattjes MP, Tintoré M, Tur C, Yousry TA, Sormani MP, et al. Evidence-based guidelines: MAGNIMS consensus guidelines on the use of MRI in multiple sclerosis-clinical implementation in the diagnostic process. Nat Rev Neurol. 2015;11(8):471–482. Cited on pages 10, 46, and 51.

[25] Multiple Sclerosis International Federation. Disease-modifying therapies for MS; 2016. Cited on page 10.

[26] Gajofatto A, Benedetti MD. Treatment strategies for multiple sclerosis: When to start, when to change, when to stop? World J Clin Cases. 2015;3(7):545–555. Cited on page 10.

[27] McRobbie D, Moore E, Graves M, Prince R. MRI From picture to proton. 2nd ed. Cambridge University Press; 2007. Cited on pages 10 and 11.

[28] Blystad I. Clinical Applications of Synthetic MRI of the Brain [Ph.D. thesis]. Linköping University; 2017. Dissertation no. 1600. Cited on page 12.

[29] Hagiwara A, Warntjes M, Hori M, Andica C, Nakazawa M, Kumamaru KK, et al. SyMRI of the Brain: Rapid Quantification of Relaxation Rates and Proton Density, With Synthetic MRI, Automatic Brain Segmentation, and Myelin Measurement. Invest Radiol. 2017;52(10):647–657. Cited on page 12.

[30] Blystad I, Warntjes JB, Smedby O, Landtblom AM, Lundberg P, Larsson EM. Synthetic MRI of the brain in a clinical setting. Acta Radiol. 2012;53(10):1158–1163. Cited on page 12.

[31] West J, Warntjes JB, Lundberg P. Novel whole brain segmentation and volume estimation using quantitative MRI. Eur Radiol. 2012;22(5):998–1007. Cited on page 13.

[32] West J, Blystad I, Engström M, Warntjes JB, Lundberg P. Application of quantitative MRI for brain tissue segmentation at 1.5 T and 3.0 T field strengths. PLoS One. 2013;8(9):e74795. Cited on page 18.

[33] Parikh R, Mathai A, Parikh S, Chandra Sekhar G, Thomas R. Understanding and using sensitivity, specificity and predictive values. Indian J Ophthalmol. 2008;56(1):45–50. Cited on page 29.

[34] Zou KH, Warfield SK, Bharatha A, Tempany CM, Kaus MR, Haker SJ, et al. Statistical Validation of Image Segmentation Quality Based on a Spatial Overlap Index. Acad Radiol. 2004;11(2):178–189. Cited on page 30.

[35] Zijdenbos AP, Dawant BM, Margolin RA, Palmer AC. Morphometric Analysis of White Matter Lesions in MR Images: Method and Validation. IEEE Trans Med Imaging. 1994;13(4):716–724. Cited on page 30.

[36] Tanenbaum LN, Tsiouris AJ, Johnson AN, Naidich TP, DeLano MC, Melhem ER, et al. Synthetic MRI for Clinical Neuroimaging: Results of the

Magnetic Resonance Image Compilation (MAGiC) Prospective, Multicenter, Multireader Trial. AJNR Am J Neuroradiol. 2017;38(6):1103–1110. Cited on page 46.

[37] Hagiwara A, Hori M, Yokoyama K, Takemura MY, Andica C, Tabata T, et al. Synthetic MRI in the Detection of Multiple Sclerosis Plaques. AJNR Am J Neuroradiol. 2017;38(2):257–263. Cited on page 46.